Research Square

Preprints are preliminary reports that have not undergone peer review.
They should not be considered conclusive, used to inform clinical practice,
or referenced by the media as validated information.

A Wss Based Hemodynamic Study on Venous Thrombosis Formation Conditions in Deep Veins

Mustafa Serdar ÇELEBİ

mscelebi@itu.edu.tr

Istanbul Technical University https://orcid.org/0000-0003-4566-0216

Hamed Pahlavani

Istanbul Technical University

Burak Yavuz

Istanbul Technical University

Research Article

Keywords: Non-Newtonian blood flow, Casson model, Bird-Carreau model, FSI, CFD, WSS indexes, TAWSS, OSI, RRT, transWSS, Patient specific DVT simulation, DVT risk assessment

Posted Date: November 3rd, 2026

DOI: https://doi.org/10.21203/rs.3.rs-11553653/v1

License: This work is licensed under a Creative Commons Attribution 4.0 International License.
Read Full License

Additional Declarations: The authors declare no competing interests.

A WSS BASED HEMODYNAMIC STUDY ON VENOUS THROMBOSIS FORMATION CONDITIONS IN DEEP VEINS

M. Serdar ÇELEBİ[†1], **Hamed PAHLAVANI**[2], **Burak YAVUZ**[1]

[1]Department of Computational Science and Engineering, Istanbul Technical University.

[2]Faculty of Mechanical Engineering, Istanbul Technical University.

Abstract. *In this study, a general simulation framework for realistic blood flow that is in continues interaction with deformable venous valve is defined and its hemodynamic performance is compared with the steady fixed valve model for different rheological viscosity models. The main objective of the proposed model is to understand the flow properties and WSS based hemodynamic mechanisms of venous thromboembolism (VTE) more specifically toward the early diagnosis of the DVT formation and its early state contains the formation of venous stasis through hemodynamic indexes. A reliable shear index-based non-invasive thrombotic risk assessment model is not available in the literature by simulating the venous stasis condition of the patient's DVT around venous valve leaflets. Based on Virchow's triad, thrombosis mostly occurs due to the existing of statis in deep vein venous valve sinus beside vessel wall injury and hypercoagulability of blood. Additionally, vessel wall deformation and resulting sinus formation behind the venous valve may also lead to systemic and local factors creating stasis conditions. For this purpose, two different flow models including steady fixed venous valve and moving venous valve (based on FSI coupling) are studied. Evolution of stress fields in longitudinal and radial directions are studied. Then, we computed Time Averaged Wall Shear Stress (TAWSS), Oscillatory Shear Index (OSI) and Relative Residence Time (RRT) based on wall shear stresses. The combined effects of WSS and circumferential stress/strain (CS) on endothelial cells (EC) due to pulsatile flow and secondary back flow in venous valve region using vascular compliance in venous return is investigated for slow and high blood velocities. Time Averaged Transverse Wall Shear Stress (transWSS) index is used for capturing the multi directional flow conditions around the venous valve sinus. Finally, Multiple combined hemodynamic index analysis is performed for the possible thrombosis formation in venous sinus region. Comprehensive verification processes of the numerical model and its validation with the analytical result for a simple cylindrical pipe geometry are presented. Results are obtained for sinusoidal pulsatile inflow condition using five different blood velocities and detail discussion on FSI results and concluding remarks are presented.*

Key words: Non-Newtonian blood flow, Casson model, Bird-Carreau model, FSI, CFD, WSS indexes, TAWSS, OSI, RRT, transWSS, Patient specific DVT simulation, DVT risk assessment.

[†]Corresponding Author: E-mail: mscelebi@itu.edu.tr
Phone: (+90) 505 424 30 15

1 INTRODUCTION

Blood flow data contain critical and valuable information for diagnosis, prognosis and earlier risk assessment of cardiovascular diseases. Veins are blood vessels responsible for carrying oxygen-poor blood from the body tissues toward the heart by venous return. Diseases of veins can be categorized into two main groups: Thrombosis formation and venous drainage. Deep Vein Thrombosis (DVT) is a medical condition characterized by forming a blood clot in deep veins combined with Red Blood Cells (RBC) and fibrins. Pulmonary embolism (PE) is a common problem among patients in intensive care units. It is known that deep vein thrombosis is the main pathologic cause for PE. DVT and PE remain today a leading health related global cause of morbidity and mortality.

Thrombosis, blocking the flow of blood through the vein usually at the cuff and the thigh, risks the patient health caused to have pain, swelling and tenderness along the distribution of the vein that brings about the importance of an immediate treat. A thrombus either arises spontaneously or is caused by clinical conditions including surgery, trauma, or prolonged bed rest and imaging techniques are clinical solutions used in diagnosing the diseases (Kyrle and Eichinger, 2005). However, recent developments in computational science and engineering (CSE) have made it possible to use numerical methods to enhance diagnostic capabilities and progress toward patient specific precision medicine regarding DVT and offer a relationship between blood flow and DVT formation.

Three-dimensional Navier-Stokes and continuity equations are used to define the blood hemodynamics using either single-phase (Sankar *et al*., 2015) or multi-phase (Wu *et al*., 2013; Aribas and Celebi, 2020) models. For the single-phase model a non-Newtonian fluid assumption is used where its viscosity changes as the shear rates changes and the non-Newtonian effect of blood could become significant when the shear rate is below 100 s^{-1} (Pedley, 1980). The shear-thinning (non-Newtonian) behavior of blood flow can also be approximated by many different models. Among them, Casson (Jung *et al.*, 2014) and Bird-Carreau (Bird *et al*., 1987) viscosity models are the most widely used ones for blood.

The term "fluid-structure interaction, (FSI)" refers to a multi-physics problem that describes the interaction between fluid flow (e.g. blood flow) and deformable structures (e.g. living tissues). There is a frequent data transfer from the flow field toward the structure field and vice versa (Bungart & Schäfer, 2006). If the governing equations of the flow and structure are solved with a single solver, it is called monolithic FSI approach (Michler *et al.*, 2003). If two separate solvers are used for two different sets of equation, this is called partitioned FSI approach (Causin *et al.*, 2005). Either monolithic or partitioned methods can be used for the problem of 3D fluid-structure interaction (FSI) in deep veins. The partitioned method can be subcategorized in weak (explicit) and strong (implicit) coupling. The weak coupling scheme, however, is not suitable for large displacement and non-uniform deformation where instability problem may occur due to lack of convergence check before advancing to next time step.

Most of FSI methods provide tree strong coupling algorithms: Fixed under-Relaxation, Aitken Adaptive Under-Relaxation (Küttler & Wall, 2008) and Interface quasi-Newton with least-squares inverse Jacobian (IQNILS) (Willcox & Peraire, 2002; Vierendeels *et al*., 2007). Among those algorithms, Aitken and IQNILS are prevailing for FSI modeling due to the fast convergence and accurate results. Some related studies (Ozkucuk, 2017) show that IQN-LS method converges much faster than Aitken's relaxation method which in turn completes the simulation in a much shorter time with the same computational resources.

There are two moving boundary algorithms used for FSI problems including the immersed boundary method (IBM) and the arbitrary Lagrangian-Eulerian (ALE). Almost all of the current OpenFOAM version of foam-extend`s FSI toolkits (e.g. `solids4Foam` and `fsiFoam`) are merely compatible with the ALE approach. Therefore, the ALE is applied for the FSI in DVT problem where the mesh requires to be frequently deformed, displaced and updated throughout time (Hirt *et al.*, 1974). The `solids4Foam` solver capable of applying Arbitrary Lagrangian-Eulerian (ALE) formulation offers a foam-extend based finite volume toolbox for solid mechanics and fluid-solid interaction simulations (Cardiff *et al*., 2018).

Earlier detection of the thrombosis formation in deep veins is merely conducted by statistical indexes based on the clinic observations. However, a wall shear stress (WSS) based specific indicator for the common DVT disease does not exist yet in the literature. But some experimental studies show that there is a close relationship among thrombosis formation, growth rates and wall shear rates (Bark *et al*., 2012). Bovill *et al*. showed that the initiation of the thrombus appears to be in the valve pocket sinus, due to its tendency to become hypoxic. Activation of endothelial cells by hypoxia or possibly inflammatory stimuli would lead to surface expression of adhesion receptors that facilitate the binding of circulating leukocytes and macrovesicles. However, endothelial cells on the surface of venous valves and inner surface of vein sinus sense the fluctuating wall shear stresses resulting from blood flow and they transform these mechanical signals to chemical signals. Wall shear stresses (WSS) have a critical importance due to both thrombus formation and vein wall-venous valve functionality beside the hypoxic feature of blood. WSS effect is mostly explained with both high and low WSS theories which lead to vascular diseases.

The purpose of this study is to construct a hemodynamic model for deep vein using Computational Fluid Dynamics (CFD) and FSI approaches to model the blood flow as a single-phase non-Newtonian flow including shear thinning feature that is in continues interaction with deformable venous valves. The proposed model is aimed to understand the WSS based hemodynamic mechanisms of venous thromboembolism (VTE) more specifically toward the early diagnosis of the DVT formation and its early states (e.g. venous stasis) through hemodynamic indexes. There are over 20 different VTE risk assessment models in literature. These models may be classified as individualized point-based scoring, and grouping or “bucket” models. None of them uses a reliable physics based evidence on patient specific hemodynamic blood flow and its interaction with the vessel wall. To the best of the Author’s knowledge, a reliable shear index-based non-invasive thrombotic risk assessment model is not available in the literature by simulating the venous stasis condition of the patient’s DVT around venous valve leaflets in different scenarios. Based on Virchow’s triad, Thrombosis mostly occurs due to the existing of statis in deep vein venous valve sinus region beside vessel wall injury and hypercoagulability of blood (Needleman, 2014). Additionally, vessel wall deformation and resulting sinus formation behind the venous valve may also lead to systemic and local factors creating stasis conditions. For this purpose, two different flow models including steady fixed venous valve and moving venous valve (based on FSI coupling) are studied. Evolution of stress fields in longitudinal and radial directions are studied. Then, we computed Time Averaged Wall Shear Stress (TAWSS), Oscillatory Shear Index (OSI) and Relative Residence Time (RRT) based on wall shear stresses. The combined effects of WSS and circumferential stress/strain (CS) on endothelial cells (EC) due to pulsatile flow and secondary back flow in venous valve region using vascular compliance in venous return is investigated for slow and high blood velocities. Finally, Time Averaged Transverse Wall Shear Stress (transWSS) index is used for capturing the multi directional flow conditions around the venous valve sinus. Multiple combined hemodynamic index analysis is

performed for the possible thrombus formation in venous sinus region. Comprehensive verification processes of the numerical model and validation with the analytical result for a simple cylindrical pipe geometry are presented.

2 MATHEMATICAL MODEL

Assuming a single-phase blood flow problem, the governing equations required to determine blood flow variables such as velocity ($\vec{u}$) and pressure (p) can be derived through conservation of mass and momentum of fluid passing through the control volume.

$$\frac{\partial \rho}{\partial t} + \nabla . (\rho \vec{u}) = 0 \tag{1}$$

Equation 1 shows the differential form of the conservation of mass (continuity equation) where ρ is the density of blood.

$$\rho \frac{\partial \vec{u}}{\partial t} + \rho(\vec{u} . \nabla)\vec{u} = -\nabla p + \rho \boldsymbol{g} + \nabla . \boldsymbol{\tau} \tag{2}$$

The momentum equation (Equation 2) is the sum of the forces acting on element of blood liquid to get its acceleration where p, $\boldsymbol{g}$ and $\boldsymbol{\tau}$ are pressure, gravity and shear stress terms respectively. Studies show that the non-Newtonian nature of blood flow does not seem to be playing a significant role in large arteries such as aorta (Pedley, 1980). But as the dimensions of the vessels get smaller and tighter the role of non-Newtonian assumption become harder to get ignored where non-Newtonian effect of flow could become significant when the shear rate is below 100 s^{-1}. Among a wide range of non-Newtonian viscosity models, the Casson and Bird-Carreau models are prevailing for investigations of shear thinning behavior of blood. The Casson model is a basic model used in blood rheology that specifies minimum and maximum viscosities (ν_{min} and ν_{max}). Beyond a threshold in strain-rate corresponding to threshold stress τ_0, the viscosity is described by a "square-root" relationship.

$$\nu = (\sqrt{\tau_0 / \dot{\gamma}} + \sqrt{m})^2 \qquad \nu_{\min} < \nu < \nu_{\max} \tag{3}$$

Equation 3 and Table 1 illustrate the Casson formulation and constants for the blood kinematic viscosity (ν) where $\dot{\gamma}$ is shear strain rate and m consistency index. Regarding the Bird-Carreua model the apparent viscosity is formulated as a function of shear rate $\dot{\gamma}$ (Perktold and Rappitsch, 1995)**.**

$$\nu = \nu_\infty + (\nu_0 - \nu_\infty)[1 + (k\dot{\gamma})^{n}]^{(n-1)/a} \tag{4}$$

where ν_0 is the viscosity at zero shear rate (Pa.s), ν_∞ is the viscosity at infinite shear rate (Pa.s), k and n are the relaxation time (s) and power index respectively.

Casson	
m	3.934986e-6
τ_0	2.9032e-6
ν_{max}	13.3333e-6
ν_{min}	3.9047e-6

Bird-*Carreau*	
ν_0	1e-3
ν_∞	1e-5
k	8.3
n	0.3568

Table 1. Casson and Bird-Carreau constants used in blood model.

2.1 Deep vein structure

As it is mentioned before, blood flow is in continues interaction with living tissues, such as vessel walls and venous valves in deep veins where it is assumed in our model for simplicity that the interaction is merely considered between blood flow and deformable venous valves attached to rigid vessel walls. The non-periodic deformation and displacement of venous valves, however, need to be achieved without adversely affecting simulation quality. On the other hand, as the nonlinearity of mathematical models gets higher and higher, so does the simulation time and the risk of failure during the process of FSI simulations. To overcome the challenges, a neo-Hookean elastic model (Cardiff et al., 2018) which is a suitable model for studying the behavior of venous valve with sudden displacement and non-periodic deformation, is used.

$$F = I + \left(\nabla_0 \vec{d}\right)^T \tag{5}$$

$$f = F.F_{[\mathrm{m}-1]}{}^{-1} \tag{6}$$

The deformation of gradient, F and relative deformation gradient, f are kinematik quantities when dealing with finite strains (Equations 5 and 6) with respect to the initial configuration where ∇_0 is gradient with respect to the initial undeformed configuration and $F_{[\mathrm{m}-1]}$ is the deformation gradient at the end of the previous time step where m represents current time step.

2.2 FSI Coupling Model

There is an exchange of information on the imaginary interface patch, and mainly this exchange is done at each time step in an iterative procedure (Matthies and Steindorf, 2003). Figure 1a describes the interaction in between fluid domain (Ω_f) and solid domain (Ω_s) sharing a common interface ($\Gamma_{f,\,s}$) and bounded by $\partial\Omega_f$ and $\partial\Omega_s$. Considering the conservation of mass and momentum, both the kinematic and dynamic continuities should be satisfied at the interface ($\Gamma_{f,s}$). The kinematic continuity states that the flow field velocity at the interface is required to be equal with the boundary velocity. Plus, according to dynamic continuity, the stresses from both fluid and solid are equal at the interface. (Equation 7 and 8).

$$u_{f,\Gamma} = u_{s,\Gamma} \tag{7}$$

$$\sigma_{s,\Gamma}.n_{s,\Gamma} = p_{f,\Gamma}.n_{f,\Gamma} - \tau_{f,\Gamma}.n_{f,\Gamma} \tag{8}$$

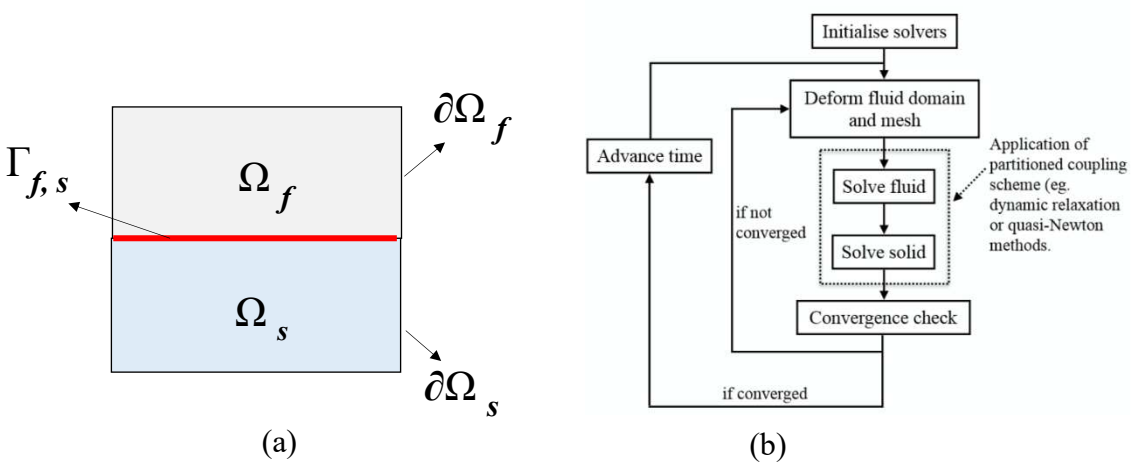


Figure 1. (a) FSI problem description, (b) strong coupling (Özküçük, 2017).

Since a strong portioned FSI approach requires to separate solvers for flow and structure fields (Figure 1b), the `solids4Foam` introduces `pisoFluid` and `icoFluid` solvers for flow field and the classic `stressFoam` for structure field, respectively as illustrated in Figure 2.

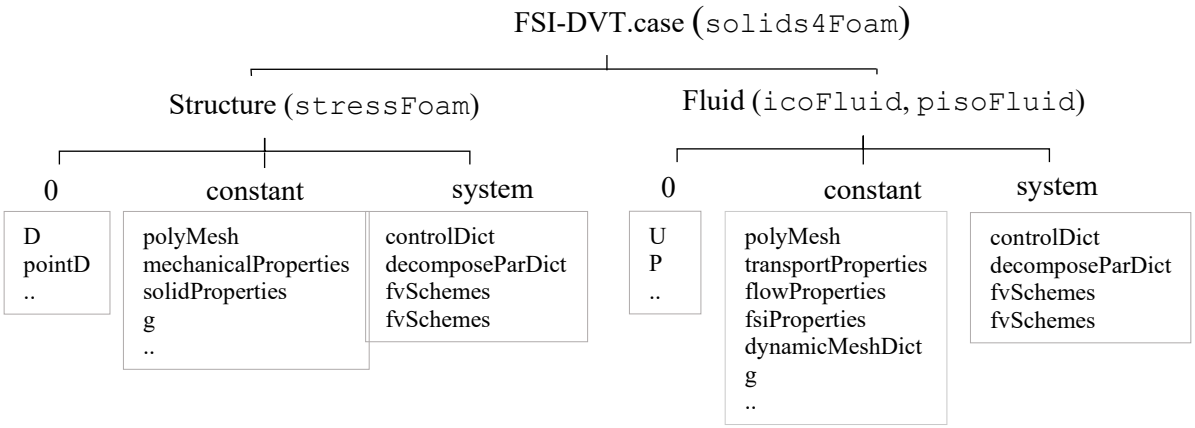


Figure 2. Directory structure of FSI in foam-extend.

3 HEMODYNAMIC INDEXES

Hemodynamic flow characteristics around venous valve sinus are further analyzed by nondimensional shear stress-based indexes each representing different complex hemodynamic aspects of flow and vessel wall responses.

Time Averaged Wall Shear Stress (TAWSS): TAWSS is one of the most prevailing hemodynamic indexes used in blood rheology that can be described as in Equation 9. Low TAWSS values (lower than 0.4 N/m^2) are known to cause vessel wall thickening that arises due to stimulation of endothelial cells lining on the vessel wall. On the other hand, high values of TAWSS values (greater that 10 - 15 N/m^2) can cause endothelial trauma, thrombus and hemolysis. Values between 0.4 N/m^2 and 10 N/m^2 are denotations of healthy vessel that is protected by any plaque formation or disorientation of endothelial cells (Syedah Salwa, 2017).

$$TAWSS = \frac{1}{T}\int_0^T |WSS| dt \tag{9}$$

We focus on both high and low values for thrombus formation at back pockets of valves, vessel wall and valve leaflet deformations.

Oscillatory Shear Index (OSI): OSI is a hemodynamic parameter that can help to define a flow as laminar (unidirectional) or oscillating (turbulent) and shows the deviation of shear stress vector from the dominant direction of blood flow during a single cycle T. It helps understanding the vascular flow characteristics. According to its definition given by Equation 10, OSI varies in a range from 0 to 0.5 and used to define regions with highly oscillating WSS. Values corresponding to 0 show that flow disruption in the vessel is minimal while values corresponding to 0.5 highlight instantaneous WSS deviates from the main flow direction in the vessel. It is also known that high OSI values may cause intimal thickening in vessel wall.

$$OSI = 0.5\left(1 - \frac{\left|\int_0^T WSS\,.dt\right|}{\int_0^T |WSS|\,.dt}\right) \tag{10}$$

It is used to identify the severe oscillating WSS regions in deep vein venous valve for potential vessel wall and leaflet thickening. In regions characterized by low shear stress may lead to favorable conditions for both plague development and venostasis (or venous stasis). OSI has also critical effects on vessel wall gene expression under reversing flow conditions (Amaya *et al*., 2016).

Relative Residence Time (RRT): RRT is inversely proportional to the magnitude of the TAWSS vector and includes effects of both TAWSS and OSI. It basically represents how long blood particles stay in a certain location. The longer the blood stays in a region, more chances of it recirculating. This recirculating blood in turns increases the probability of platelet aggregation leading to thrombus formation and stroke.

$$RRT = \frac{1}{(1-2OSI)TAWSS} = \frac{1}{\left|\int_0^T WSS\,.dt\right|} \tag{11}$$

We use RRT to identify the elevated temporal residence of blood flow at pocket region of the venous valve.

Time Averaged Transverse Wall Shear Stress (transWSS): transWSS index gives a more effective definition in defining multi directional flow characteristics. In Equation 12, we calculated the time dependent mean by considering the non-zero WSS components in the normal direction to the vector.

$$transWSS = \frac{1}{T}\int_0^T \left|\tau_w\left(n \times \frac{\int_0^T \tau_w\, dt}{\left|\int_0^T \tau_w\, dt\right|}\right)\right| dt \tag{12}$$

It is known that the pattern of transWSS is relatively insensitive to inflow flow characteristics while sensitive to changes in vessel geometry and valve displacements. Since transWSS calculates the average over the one cycle of WSS which is perpendicular to the temporal mean WSS vector, endothelial cells are affected by cross flow (Wang *et al.*, 2013) as a result of reverse secondary flow.

4 Numerical Simulations and Validations

A set of verification and validation steps are conducted for evaluating the accuracy and reliability of the model. First grid convergence analysis is used for velocities at the selected cross section. For this, a non-Newtonian blood flow model is considered inside a horizontal cylindrical pipe (see in Figure 3) where its diameter (D) and length (L) are 0.02m and 0.4m respectively. Blood is assumed as homogeneous, isothermal and incompressible fluid. Uniform velocity profile (U_z) in longitudinal direction passing through cross-sections A, B and C is measured under laminar flow conditions. For a grid convergence (GCI) study, model is run with various mesh sizes 35k, 70k, and 105k and results are compared in Figure 4 for inlet velocity 0.45 m/s. Based on the model simulation results where velocities are measured at section C, $70x10^3$ mesh elements are fine enough to capture velocity magnitudes in the simple flow domain. Two viscosity models (Casson and Bird-Carreau) are tested in the same benchmark geometry for four uniform inflow (0.10 m/s, 0.20m/s, 0.30m/s and 0.45m/s) velocities. Typical shear thinning feature of blood modelled by viscosity models is observed on velocity profiles.

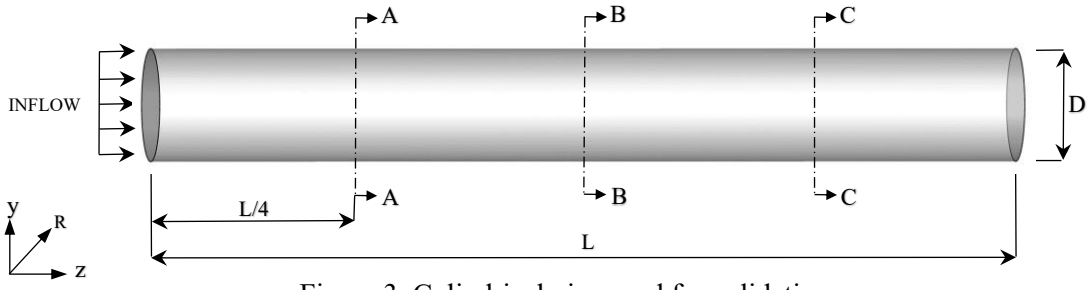


Figure 3. Cylindrical pipe used for validation.

Uniform blood flow passing through cross-sections A, B and C is plotted in Figure 5 for two shear thinning models. Results show that difference between two models is higher at low velocities and closer at higher velocities. In other words, if flow is momentum dominated then shear-thinning effect starts to decrease and viscosity models generate similar shear-rate viscosity interaction. We also observe in Figure 5 how flow develops along the pipe and the difference between two viscosity models slightly reduces at low velocities. Key question here which viscosity model is over estimate or under estimate the velocity especially at low velocities. To justify this we compared the non-Newtonian numerical model which uses Casson approximation with the analytical result. A different sized horizontal

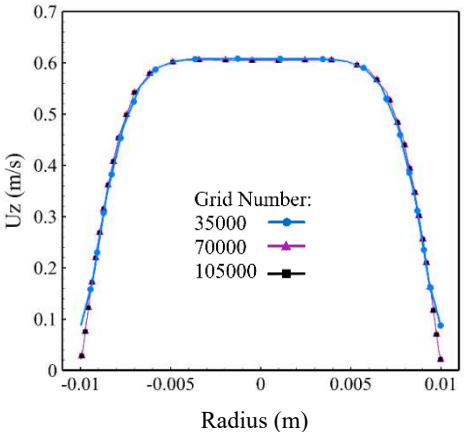


Figure 4. Grid convergence analysis for the velocity profile at the section C with an inlet velocity of 0.45m/s.

cylindrical pipe given in Figure 6 is selected for the validation of the Casson viscosity model. Uniform velocity profile (U_z) in longitudinal direction passing through cross-section A is

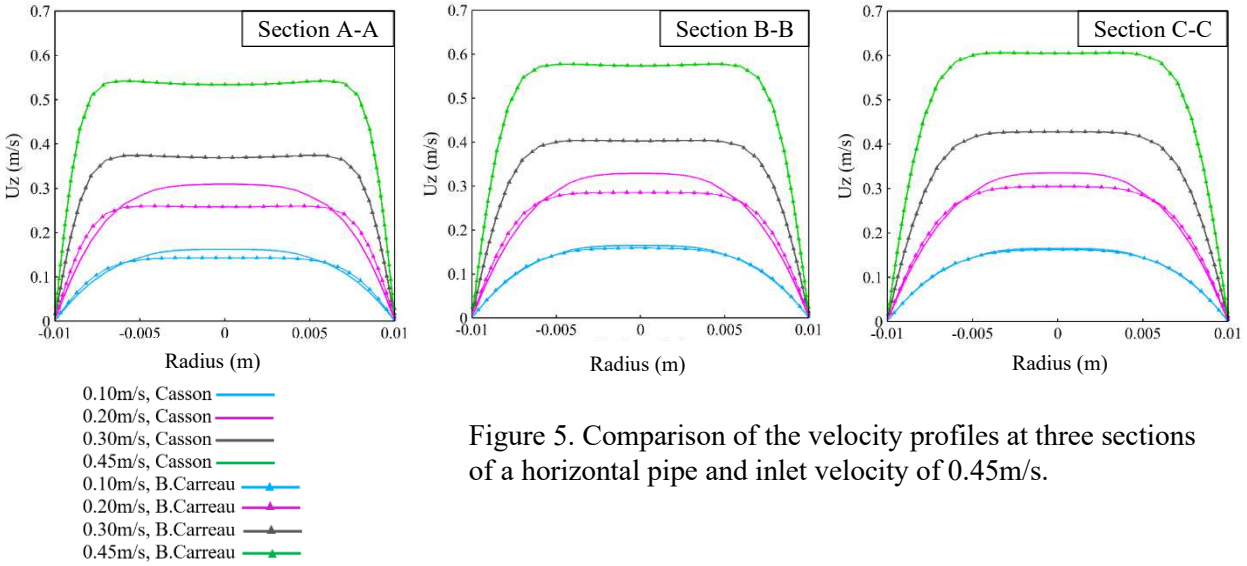


Figure 5. Comparison of the velocity profiles at three sections of a horizontal pipe and inlet velocity of 0.45m/s.

measured under laminar flow conditions. A transient blood flow is used for solving the continuity and momentum equations of the laminar flow through the PISO algorithm for three different uniform inflow blood velocities (0.05 m/s, 0.1m/s and 0.2 m/s).

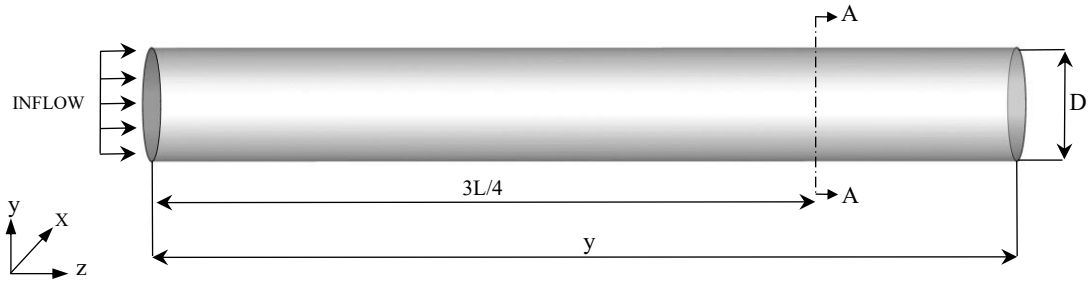


Figure 6. Cylindrical pipe used for the validation of Casson viscosity model.

Results in Figure 7 show close correlation with the analytical results of Mazumdar J.N. (2004) regardless of blood velocity. Our CFD results are slightly smaller than analytical results and get flat tendency near to mid-section of the pipe reflects the shear-thinning behavior.

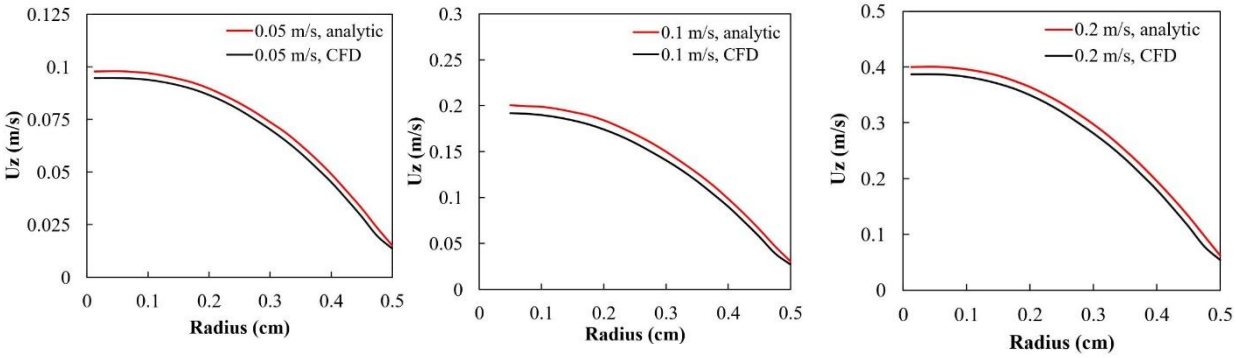


Figure 7. Comparison of analytical and our CFD results for three different velocities.

Above results support that model has a mesh independence and Casson viscosity model used has a close correlation with the analytical solution. We extended this verification and validation process to our actual simulation scenario including venous valve leaflets and sinus region in a deep vein geometry as seen in Figure 8. In order to obtain the most appropriate grid size and number, grid convergence analysis (GCA) is implemented by generating the series of grids that can vary from course to fine spacing. Four grids with 4×10^5, 6×10^5, 8.5×10^5 and 1.6×10^6 mesh elements are used to approximate to the velocity along the sinus region. Figure 9 compares grid convergence results for velocities at three sections for inlet velocity of 0.30m/s. It is seen that velocities at high and low gradient zones are aligned after grid number $8.5x10^5$.

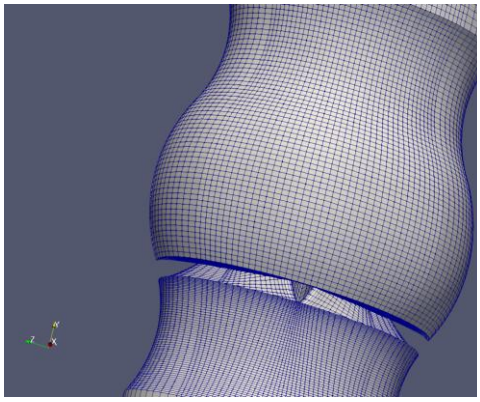


Figure 8. Deep venous geometry.

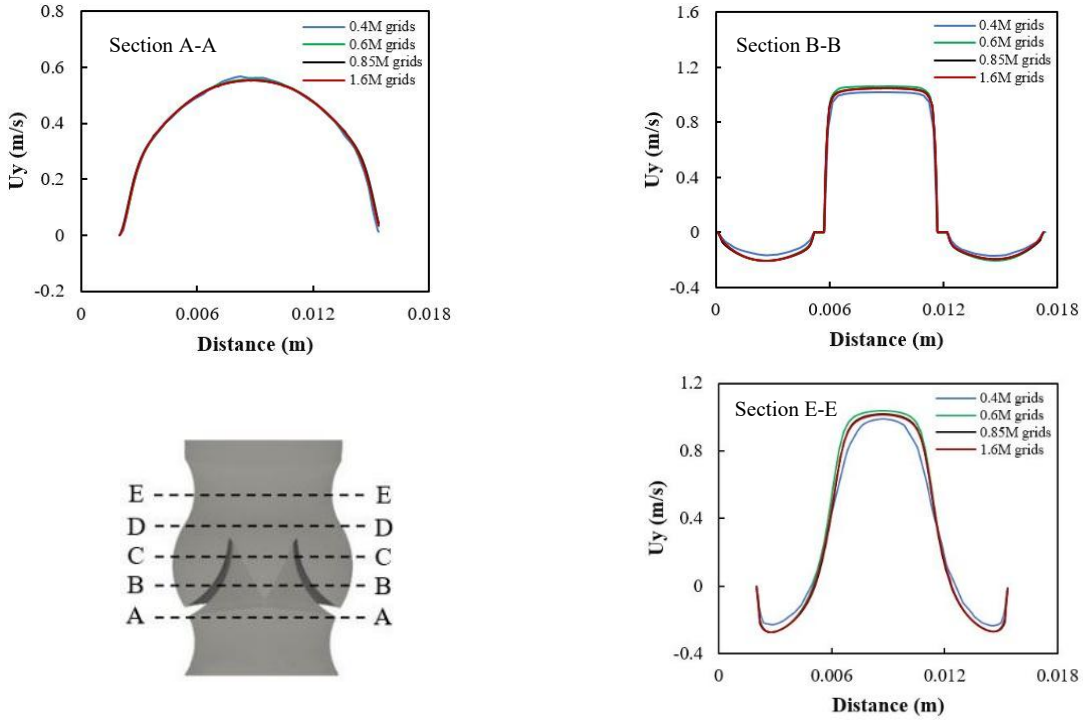


Figure 9. Grid convergence analysis for the velocity profiles at three sections and inlet velocity of 0.30m/s.

Finally a residual analysis is performed for deep vein and venous valve simulation to observe that critical flow parameters are converged under the acceptable error limits. Figure 10 shows the converged results of velocities and pressure during the solution process of p-v coupling of Navier-Stokes equations with the continuity equation. Based on the verification and validation results, we conclude that our blood flow model has a capability of generating consistent results with an acceptable level of accuracy.

4.1 Hemodynamic Modelling of the DVT Problem

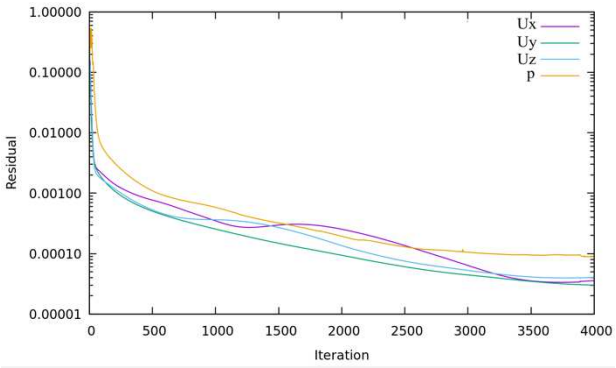


Figure 10. Residual analysis of velocities and pressure in deep vein venous valve simulation.

Well known Virchow's triad proposes that thrombosis occurs due to the existing of stasis, vessel wall injury and hyper-coagulability. In this work, we focus on the investigation of stasis condition leading to a DVT frequently begins in the valve sinus zones of deep veins. Blood stasis is a thrombogenic stimuli in pathogenesis of venous thromboembolism. Systemic and local are two major factors creating stasis conditions in deep veins. Systemic factors mostly result from immobilization pools blood in venous sinuses and increased blood viscosity. The blood flow pattern in the venous valves can cause low oxygen concentrations (hypoxemia) in the valve sinus.

As the local factor, hypoxia of venous valve cusps produces tissue factor and activates coagulation process and additionally accumulation of clotting factors occurs in venous sinus pockets. Despite the fact that many in vivo observations require the consideration of interaction between flow field and living tissues such as vessel wall and venous valve, conducting numerical simulations merely upon the flow field with a fixed (rigid wall) geometry can be beneficial in limited ways. In this section, we will stress the importance of FSI modelling in DVT compared to the rigid wall approach and discuss a hemodynamic simulation based DVT risk assessment mechanism under the light of various hemodynamic indexes. Highly oscillating flow fields require unsteady flow analysis which can be coupled with structure deformation. For this purpose, an open-source code `solids4Foam` is used which employs `pisoFluid` and `solidFoam` solvers for modeling the unsteady non-Newtonian single-phase blood flow and deformable venous valve leaflets. The time dependent results coming from FSI analysis would help us to understand the importance of blood flow and venous valve coupling on the assessment of stasis and thrombus formation in DVT and VTE.

4.1.1 Deep Vein Geometry

The deep vein geometry shown in Figure 11 consists of vessel wall, venous valves, inlet and outlet zones, in which its length (l) and diameter (d) are 0.2m and 0.015m respectively. Keeping the rigid wall assumption in mind, two different valve openings are considered for the laminar steady flow simulations. Wide and short span venous valve openings are selected as 34° and 15° respectively. Accuracy and convergence rates are the most critical factors in CFD simulations, and both are highly dependent on the grid generation strategy. A full hexahedral mesh generation in multi-block structured topology is used which allows the user to generate hexahedral grids of higher resolutions.

The deep vein geometry and its mesh construction strategy for transient FSI model shown in Figure 12 look much the same as they used for steady DVT cases. The structure domain, however, is required to be included for coupled structural analysis. As it was mentioned earlier, an interface is

essential for two-way data transfer from fluid domain to solid and vice versa. Additionally, conducting many initial strong couplings on the valve geometry shows that the iteration performance and additional cost of FSI are heavily dependent on the mesh accuracy and quality. The same block structure mesh generation tool seems to be the one of the best solutions for a few reasons. First and most importantly, `solids4Foam` (a solver used for FSI) provides three methods for transferring information between the coupled interfaces which are direct map, radial based function (RBF) and general grid interface (GGI) methods. Among them direct map method gives the best option for our case to minimize the risk of simulation instability.

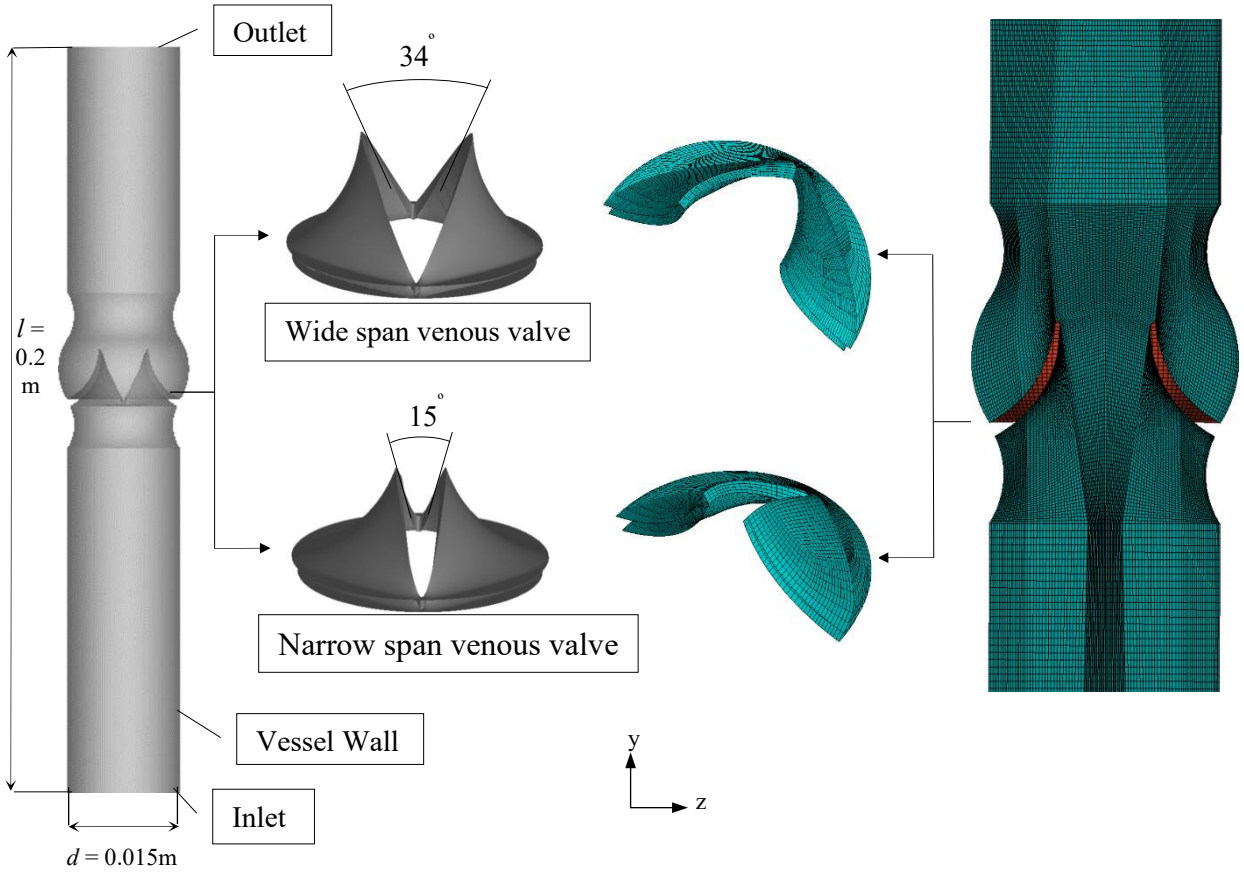


Figure 11. Deep vein of the lower extremity; Geometry and grid structure for rigid wall.

Because the application of direct map data transfer method is merely possible if the interconnecting meshes from two physical domains become conformal (the intersection between any two elements is a sub-element of both; a face, and an edge) at the interface. Secondly, considering the overall deformation of the valve's leaflets, one can easily predict the most suitable mesh order for covering the ALE method. Mesh resolution is increased in the sinus and valve regions to capture the hemodynamics flow characteristics better. Venous valve geometry in Figure 12 is combined with both fluid mesh and structure mesh and unified mesh structure is generated. Fluid mesh domain is a dynamic mesh domain and move with the valve leaflets. Mesh sizes of both domains should be in the same or close sizes for the efficient mapping.

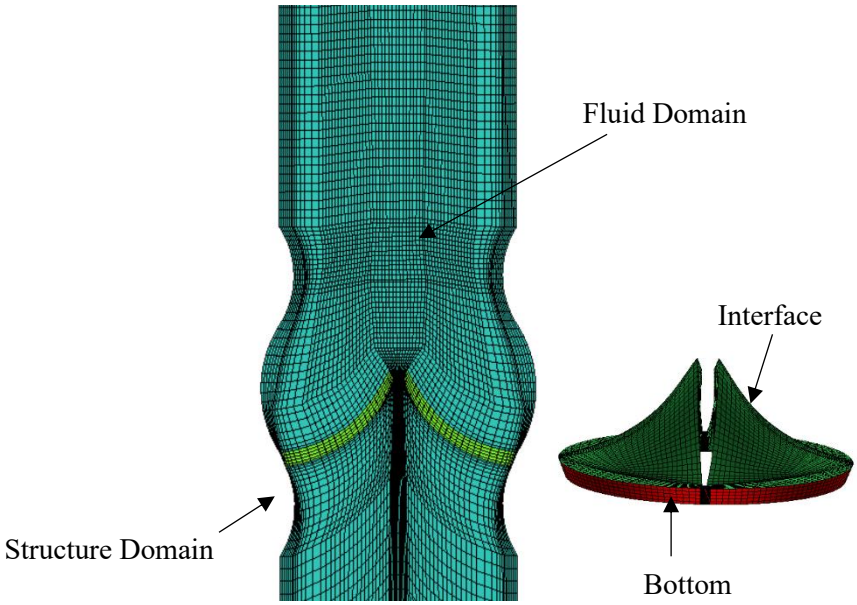


Figure 12. Deep vein geometry. Blood and valve domain's mesh structure for FSI.

4.1.2 Numerical schemes and Boundary Conditions

The finite volume method (FVM) is used as the discretization method for the approximate solution of Navier-Stokes and continuity equations. Both steady fixed and transient unsteady FSI simulations are run on clusters (50 cores @ each node) with OpenFOAM software. Sinusoidal periodic simulations run for two periodic cycles to dissipate initial transient flows. The `simpleFoam` and `pisoFoam` solvers for steady and transient flows are used with the SIMPLE algorithm (Weller *et al.*, 1998) to model the incompressible blood flow. Since our numerical investigations concern the hemodynamic conditions leading to a DVT particularly for the patient`s standing position, the gravitational acceleration term (g) is considered as opposite to flow direction. Consequently, five different blood velocities (0.05, 0.1, 0.2, 0.3 and 0.45 m/s) are used as the uniform inflow velocity condition. Table 2 shows the general forms of boundary conditions used for the steady state CFD analysis. In the model k and ε are taken as 0.03 and 0.4 at the inlet and zero gradient at the outlet.

Patch Name	U	p	k	ε
Inlet	fixedValue	zeroGradient	fixedValue (0.03)	fixedValue (0.4)
outlet	zeroGradient	fixedValue (0)	zeroGradient	zeroGradient
Venous.Valves	noSlip	zeroGradient	kqRWallFunction(0.03)	epsilonWallFunction(0.4)
Vessel.Wall	noSlip	zeroGradient	kqRWallFunction(0.03)	epsilonWallFunction(0.4)

Table 2. Boundary conditions used for steady flow and rigid wall model in DVT.

Patch Name	U	p
Inlet	Sinusoidal-Profile	zeroGradient
Outlet	zeroGradient	fixedValue (0)
Interface	movinWallVelocity	zeroGradient
Vessel.Wall	noSlip	zeroGradient

Table 3. Boundary conditions used for unsteady flow FSI analysis in DVT.

Patch Name	DD	pointDD	Young Modulus(E)	Poisson Ratio (nu)
Bottom	fixedDisplacement	fixedValue	1Mpa	0.45
Interface	solidTraction	calculated	--	--

Table 4. FSI boundary conditions used for deformable structure analysis in DVT.

Tables 3 and 4 show boundary conditions used in FSI modelling of unsteady blood flow and deformable venous valve leaflets. Unlike the steady blood flow cases, harmonic oscillating (sinusoidal wave) inlet velocities (U_{inflow} = 0.1 and 0.2 m/s) are used as given in Figure 13. At the outlet patch, zero pressure boundary condition is implemented. The valve and its leaflets are encastered to inner face of deep vein sinus wall and their tips are free to move with the blood velocity. Inflow blood flow period T_b is taken as 2 s.

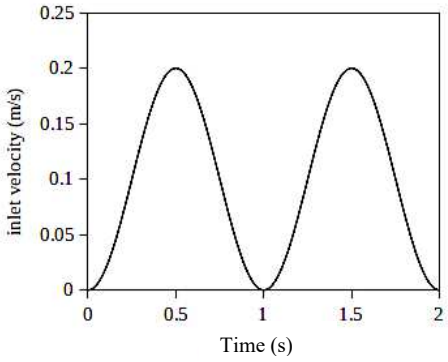


Figure 13. Sinusoidal inlet blood velocity with 0.2 m/s maximum amplitude.

4.1.3 Analysis of Blood Flow Patterns

The blood flow pattern analysis of deep veins based on rigid wall assumption has been discussed in the literature (Parimi, 2010; Aziz *et. al*., 2015). However, there are substantial differences between certain hemodynamic flow characteristics of the rigid wall/valve and FSI models which will be discussed in this section. Steady fixed-wall model is a simple model providing fast and time independent results excluding transient effects which may include critical hemodynamics flow features in deep vein. As a first step, we identified these features by simply running the steady model with the same boundary conditions of FSI model.

For non-Newtonian uniform flows, Reynolds number (Re) and inflow field is kept constant in a consistent way to maintain the same inertia and momentum. Figure 14 shows the evolution of shear stress with respect to inertia for uniform flow at three Reynolds numbers (Re = 300, Re = 650 and Re = 1274). Results show that the shear stress magnitude increases with inertia especially in sinus zone and above, but there always exist areas of very low shear stress below the venous sinus, recirculation and exit zones (seen in Figure 14a), while high stresses are generated in the recirculation boundaries, located in the side walls (seen in Figure 14b). Such distribution induces

high stress gradients and the possibility of shear stress oscillations, in space and time, which may facilitate the inflammatory process and the triggering of an atherosclerotic plaque. But blood velocity and pressure are mostly low in deep veins, thus risk factor of observing inflammatory process and plaque formation is limited.

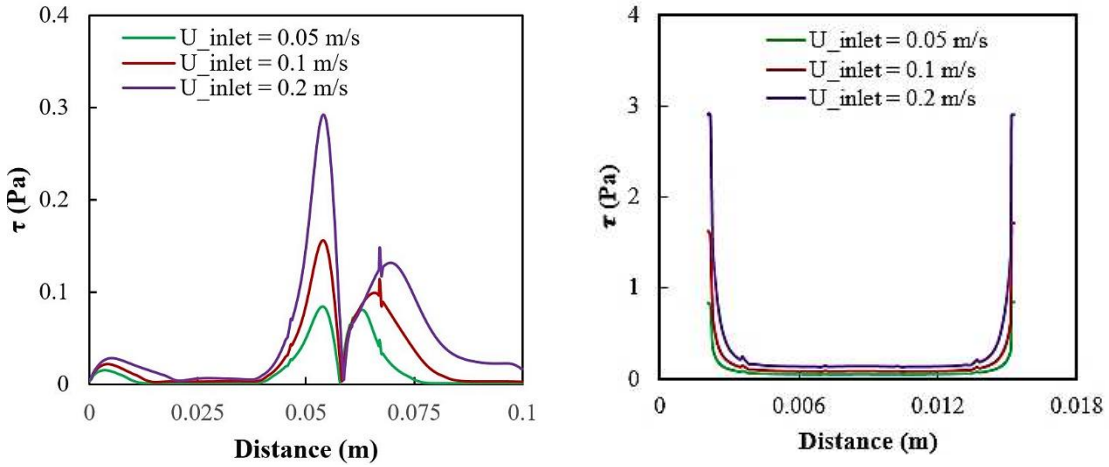


Figure 14. Evaluation of shear stress field with increasing Reynolds numbers for uniform flow of fixed wide-open valves. a) Longitudinal middle line, b) horizontal middle line.

Figure 15 shows the evolution of shear stress field with harmonic oscillation flow for various Reynolds numbers (Re = 330, Re = 670 and Re = 1285, measured at peak velocity). The flow rate ratio promotes an increase of maximum shear stress magnitudes specifically along the sinus and secondary flow zones. The higher shear stresses are observed on the inner wall layers along the deep venous sinus region. The maximum magnitudes occur where flow layers of fluid having high and low velocities come into contact, which results in increased local shearing of the blood flow.

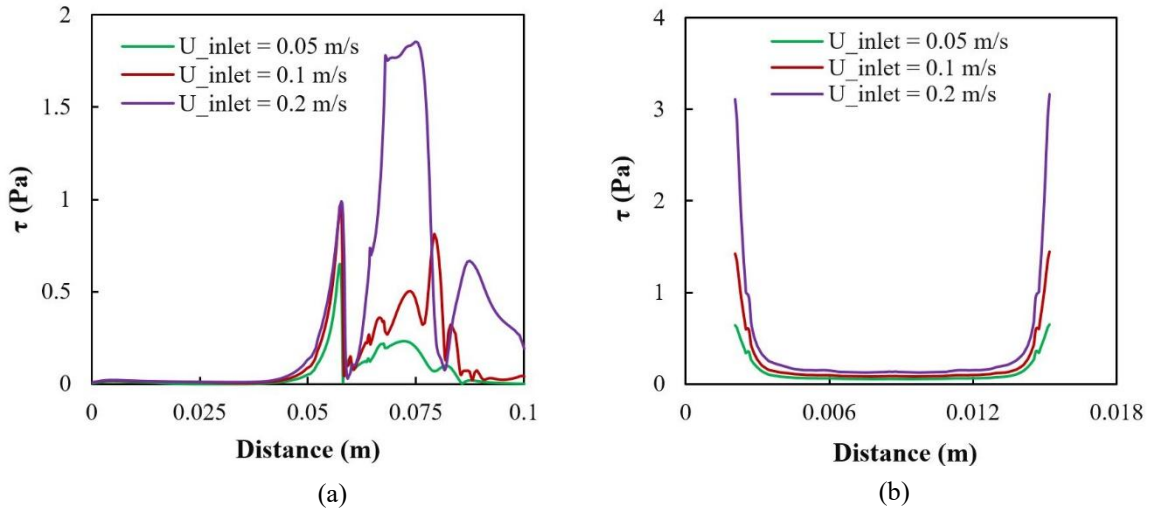


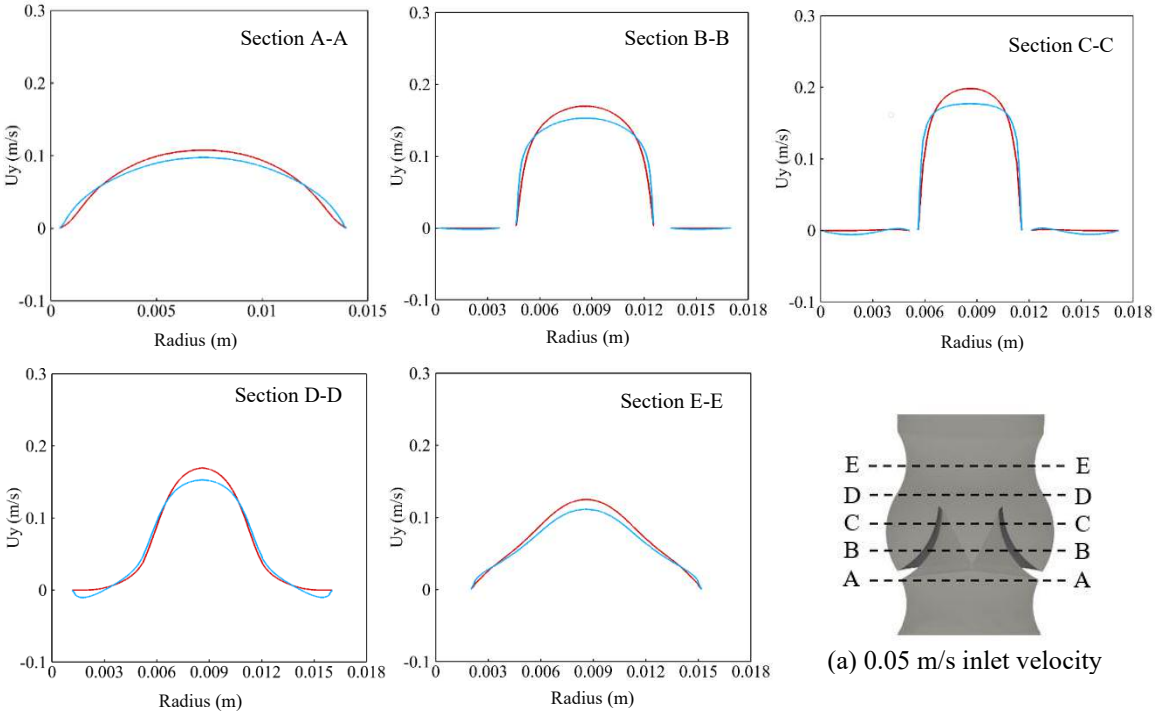
Figure 15. Evalution of shear stress field with increasing Reynolds numbers for harmonic oscillation (sinusoidal) flow of FSI. a) Longitudinal middle line, b) horizontal middle line.

For unsteady FSI flows, blood velocity promotes significant variations in the shear stress fields seen in Figure 15a compared to steady fixed valve flows. This difference goes up to six times higher than the steady case for 0.2 m/s blood velocity as expected. Shear stress field in fixed valve case has two peaks and biggest one occurs at the valve location then second peak follows it at the upper sinus exit (Figure 14a). Shear stress variations are monotonous in fixed valve case as expected, however in FSI case, these variations are significantly higher and diverse in terms of spatial positions and magnitudes. Main difference results from the fact that FSI case spans all valve leaflet closing angles and include narrow openings which may generate high blood velocities leading to bigger shear stress deformations. In this way, FSI model captures full span of hemodynamic characteristics and rheology of blood flow interacting with the venous valve deformable leaflets. Sudden jump in shear stress field for 0.2 m/s inlet velocity shows highly nonlinear interactions of blood flow with both secondary reverse flow and narrowing sinus exit.

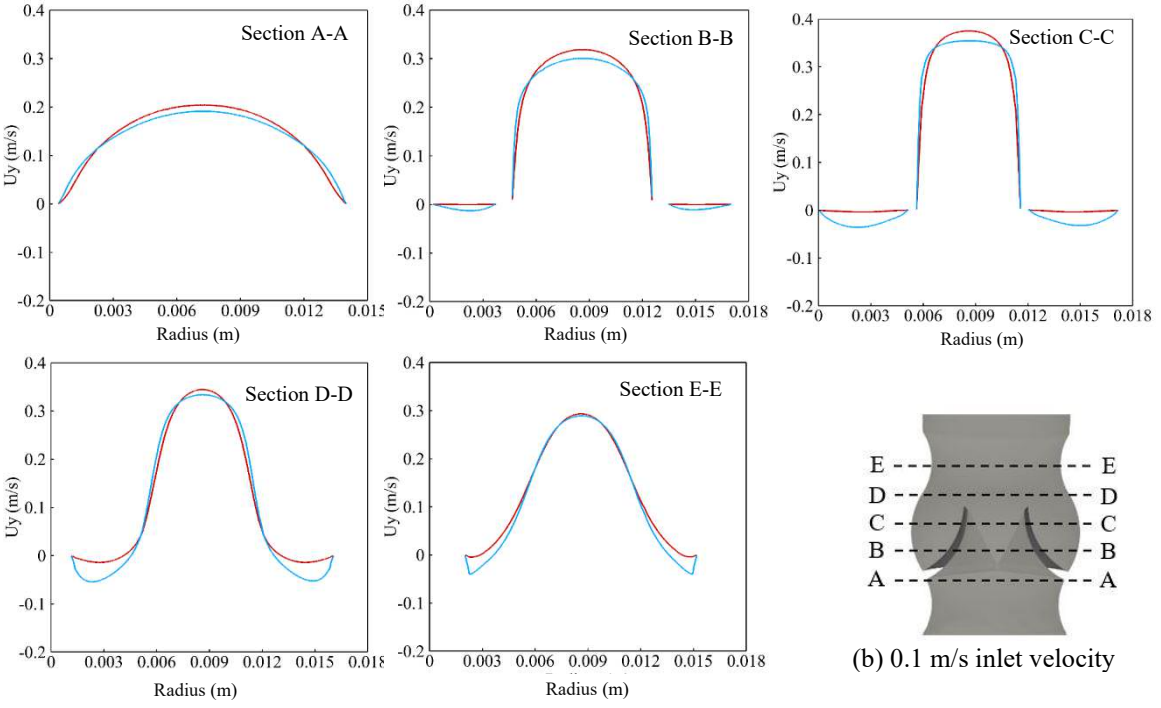
The effect of non-Newtonian rheology in the flow field is investigated and axial velocity profiles (U_y) for five different velocities from slow to high on the symmetry plane of deep vein and valve sinus region are presented in Figures 16 and 17 for two viscosity models (Casson and Bird-Carreau) and two valve spans.

In general, form of the velocity profiles around the valve sinus sounds to be identical for both viscosity models. Bird-Carreau model predicts higher values especially where the valve cusps are parallel right at the middle of the valve opening. At all velocities, differences occur between viscosity models both at the valve outlet where the velocity at its highest level and valve back zone where the velocity at its lowest level. At higher inflow velocities, bigger differences occur at the back pocket of the valves where velocities are very slow and mostly derived by the secondary flow. Similarly, at higher velocities differences tend to decrease both at all sections (from A to E) and valve openings due to the inertia dominated flows. Maximum differences between two viscosity models are observed at the back pocked of the venous valves at 0.2 m/s velocity. Previous theoretical comparison in the above section showed that shear thinning velocity profile of blood flow better captured by Casson viscosity model. We compared at the validation section that Casson model has a close estimate with the analytical results. Therefore, it is fair to say that at high velocity regions, Bird-Carreau model gives over-estimate velocities, on the other hand, at back pocked region of valve where low velocities observed Bird-Carreau gives under-estimate results. Casson model also captures the secondary back flow better than Bird-Carreau model which will be discussed at the following sections.

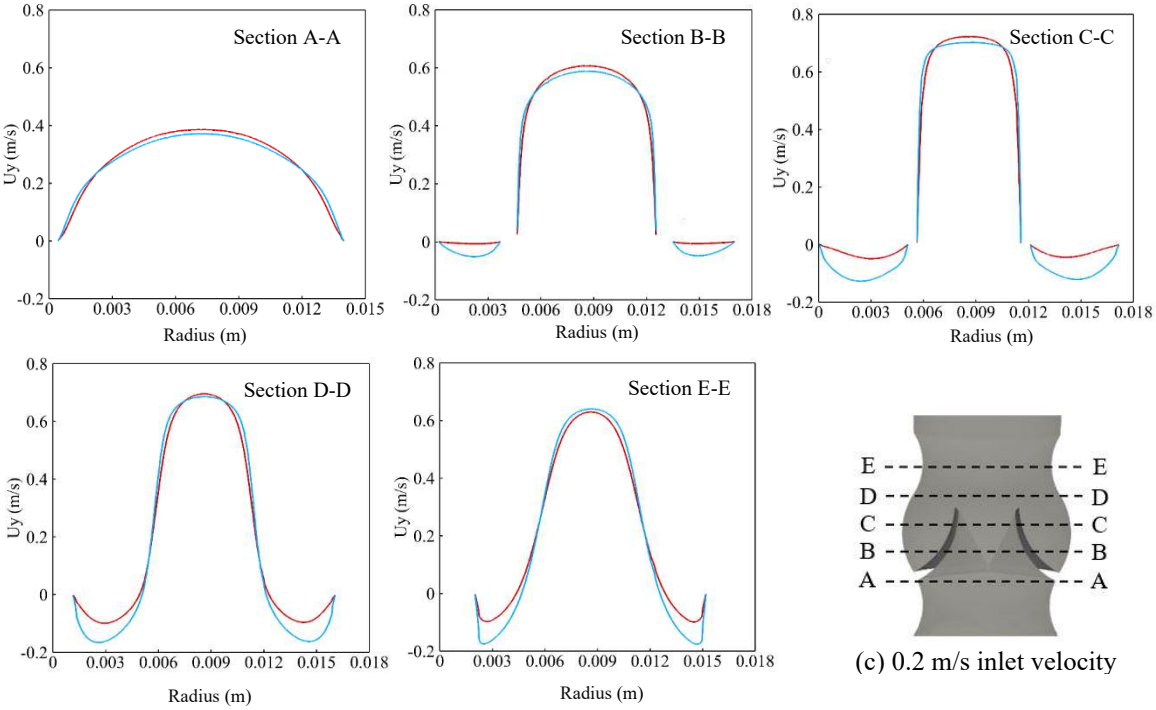
For all cases in wide span opening, maximum velocities occur at sections C and D. However in narrow span cases, maximum velocities occur only at section C. When the valve span size gets wider, the local velocities around valve and sinus region becomes smaller. Secondary flow velocities at back pocket region increase with the increasing velocities at short span opening.



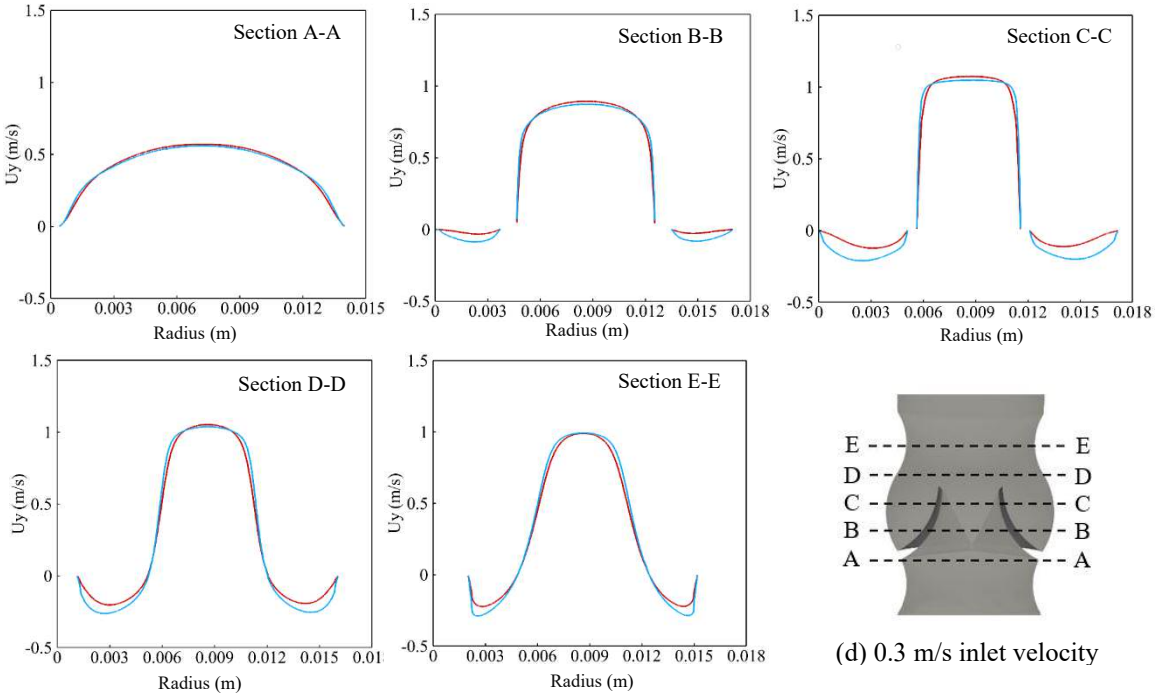
(a) 0.05 m/s inlet velocity



(b) 0.1 m/s inlet velocity



(c) 0.2 m/s inlet velocity



(d) 0.3 m/s inlet velocity

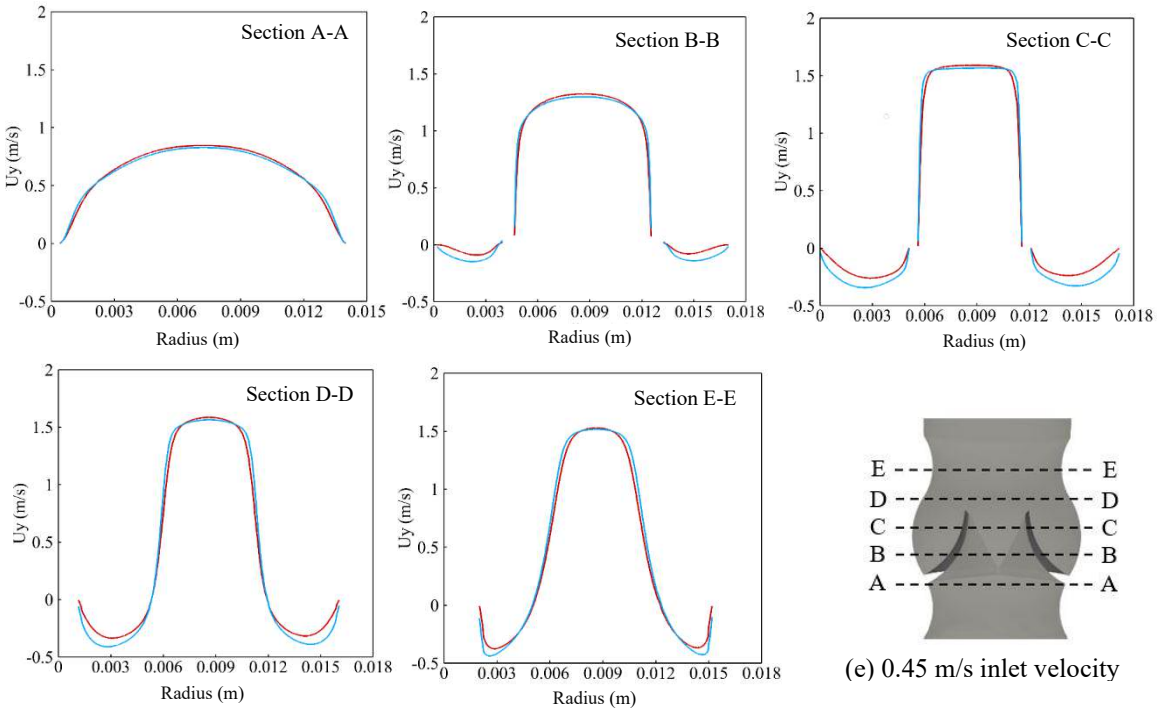
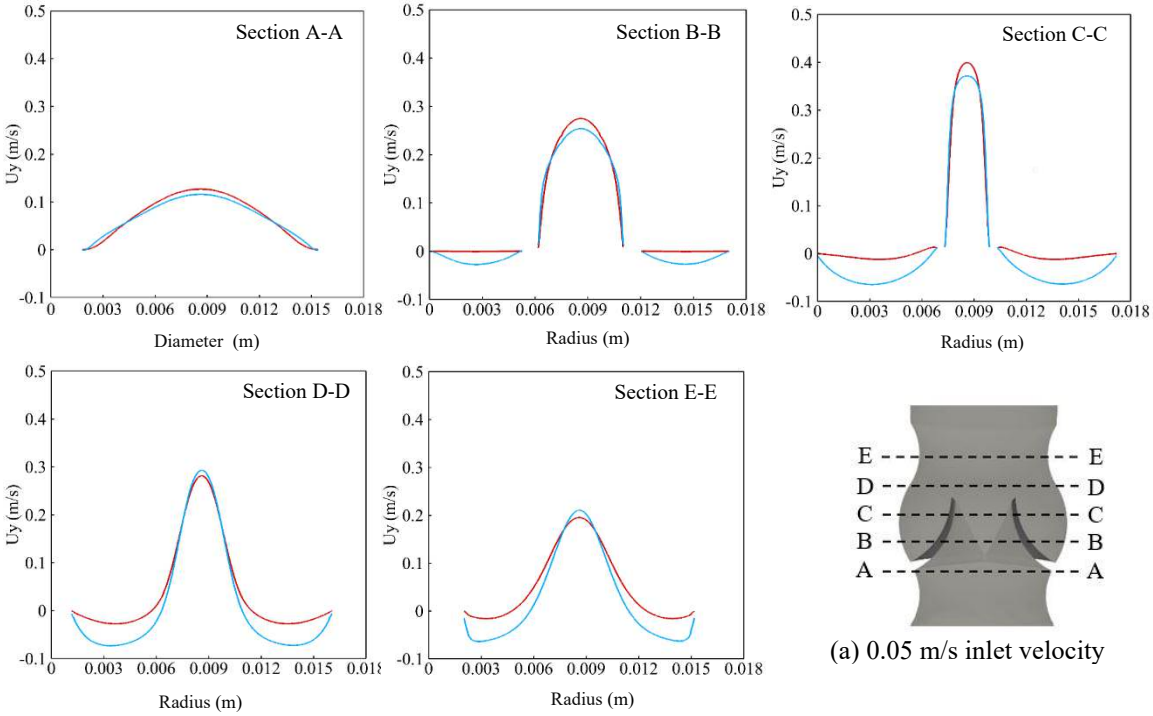
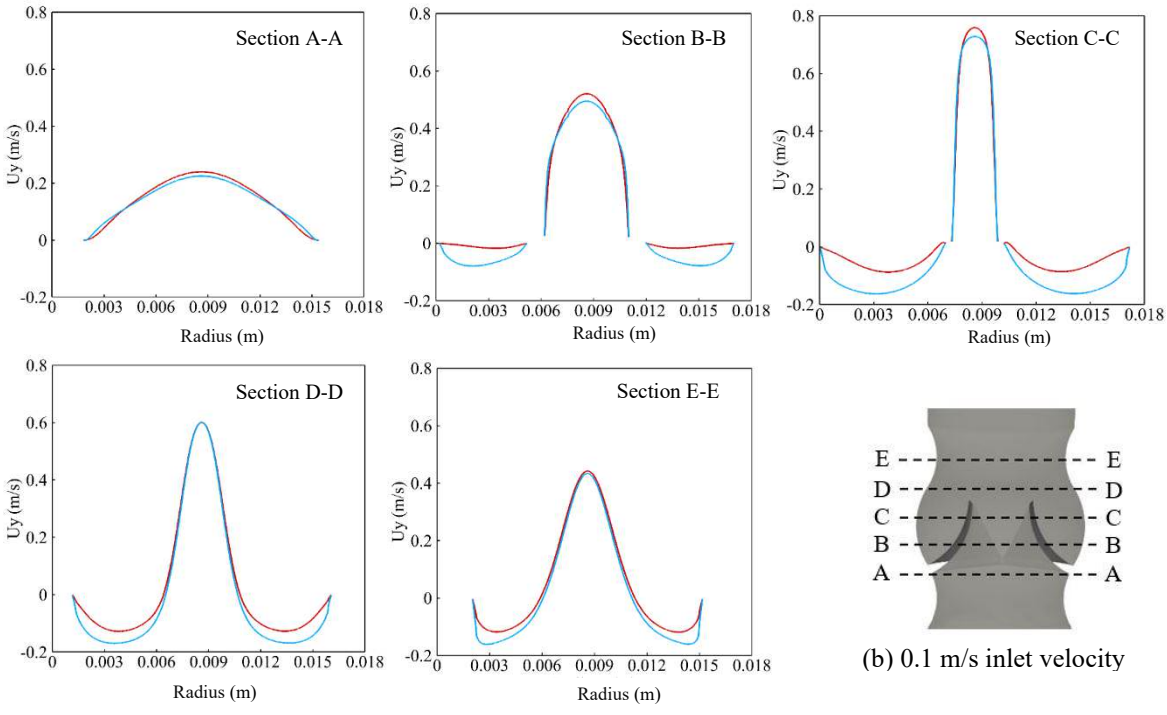


Figure 16. Velocity profiles for Casson (—) and Bird-Carreau (—) viscosity models at A, B, C, D, E sections with (a) 0.05 m/s inlet velocity, (b) 0.1 m/s inlet velocity, (c) 0.2 m/s inlet velocity, (d) 0.3 m/s inlet velocity and (e) 0.45 m/s inlet velocity for wide span valve.

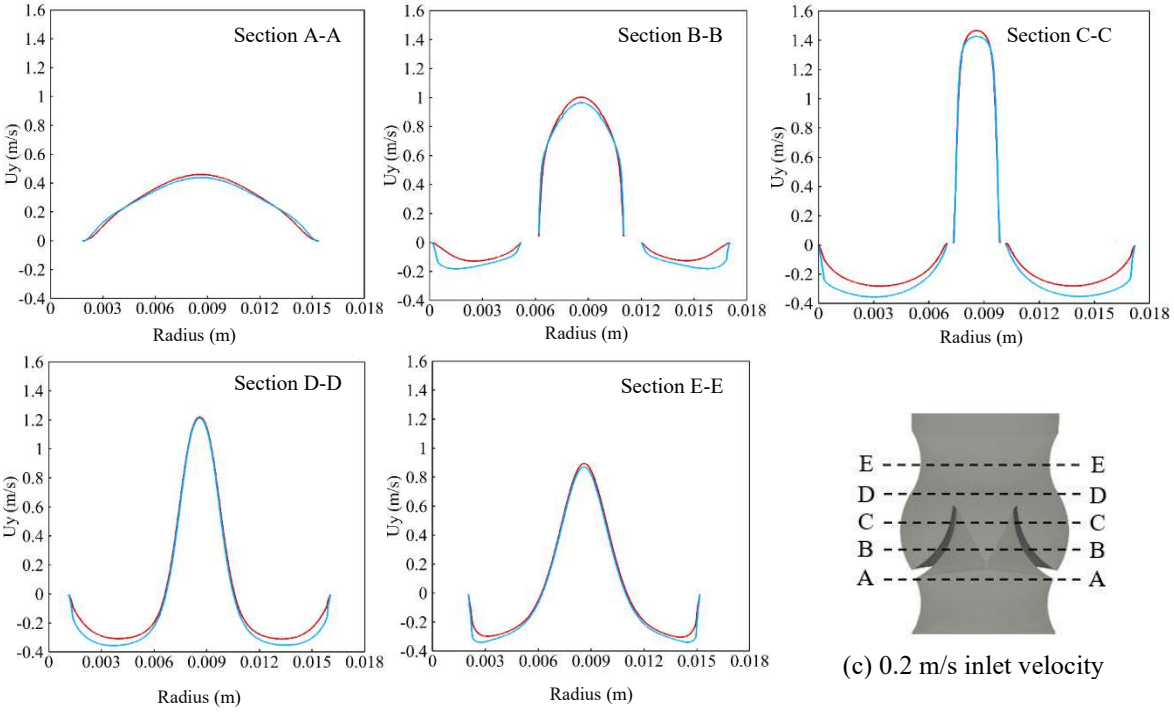
For short span opening of venous valve, velocity magnitudes increase and reaches to farer region which is close to the exit zone as expected. This causes that flow separation occurs away from the sinus region and extend the length and magnitude of the secondary/back flow which is critical for hemodynamic characteristics of the venous blood flow. Maximum differences between two viscosity models for short span opening occur at lower blood velocities such as 0.05 and 0.1 m/s. Locations of these differences occur again symmetric back pockets of valve mostly fed by secondary back flow.



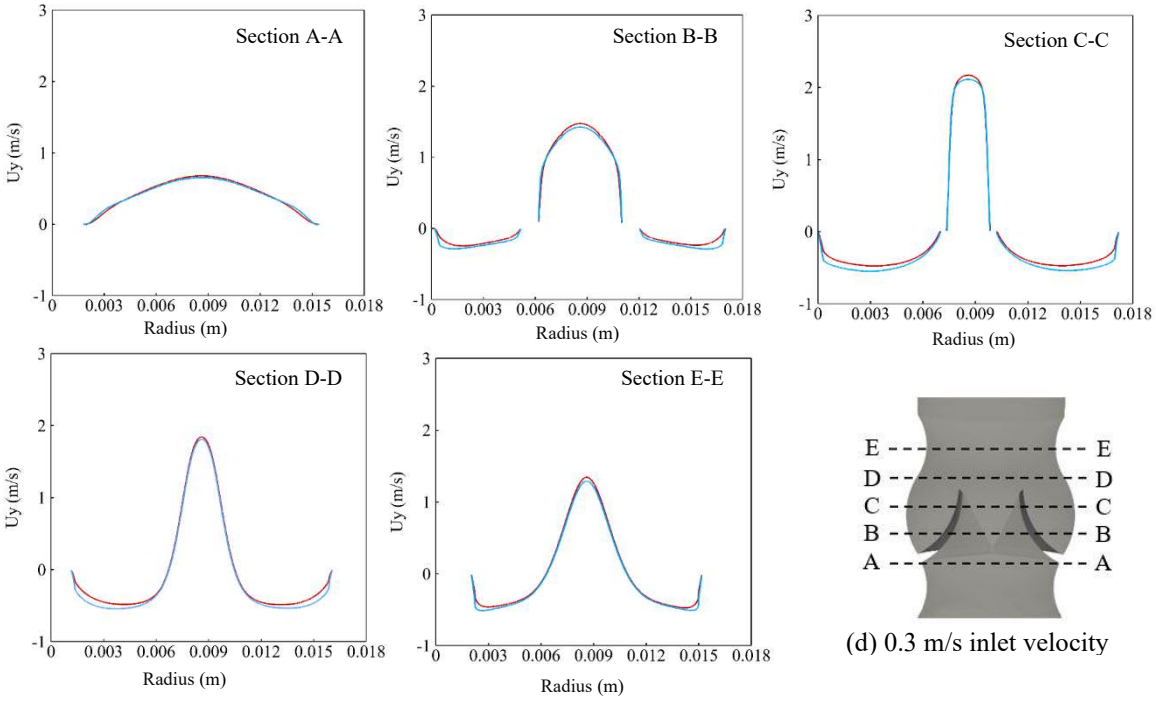
(a) 0.05 m/s inlet velocity



(b) 0.1 m/s inlet velocity



(c) 0.2 m/s inlet velocity



(d) 0.3 m/s inlet velocity

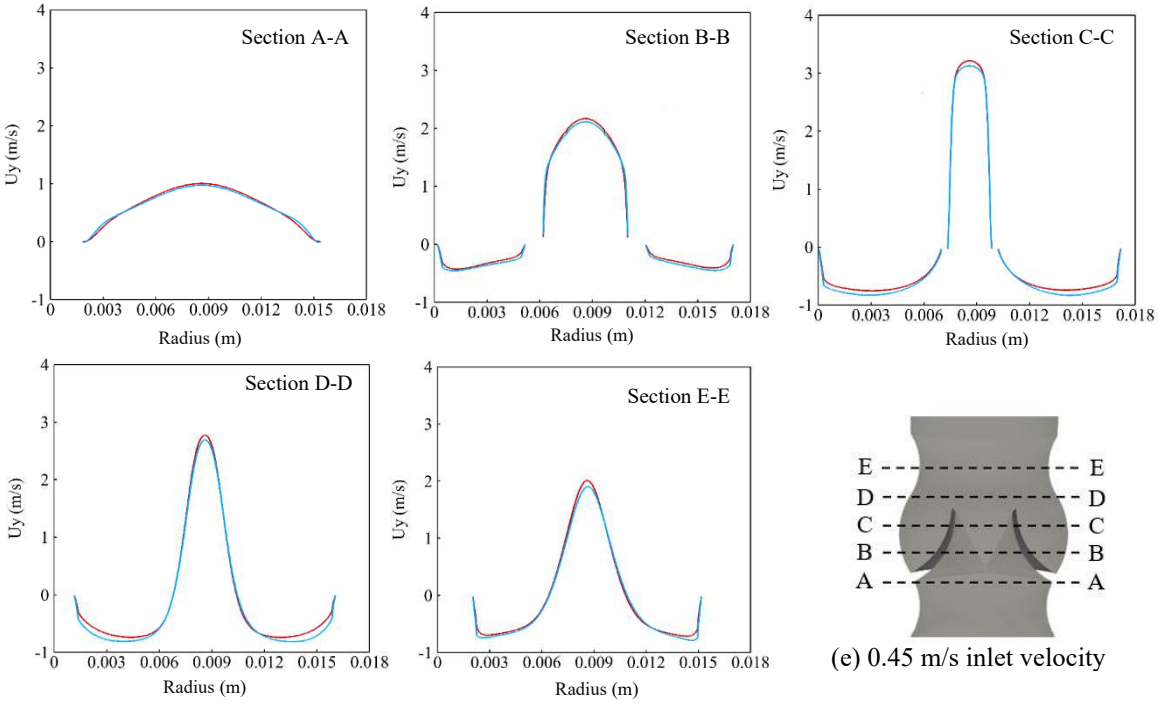


Figure 17. Velocity profiles for Casson (—) and Bird-Carreau (—) viscosity models at A, B, C, D, E sections with (a) 0.05 m/s inlet velocity, (b) 0.1 m/s inlet velocity, (c) 0.2 m/s inlet velocity, (d) 0.3 m/s inlet velocity and (e) 0.45 m/s inlet velocity for short span valve.

Clinic evidences suggest that initiation and progression of atherosclerotic disease is influenced by disturbed flow including flow separation, low oscillatory wall shear stress, high shear stress zones, reverse/vortical flows and long fluid particle residence times. Back zone of the venous valve shown in Figure 18 is known as the parietal zone (back pocket) and referred as the most critical area for clot formation due to a simultaneous flow circulation with long residence times.

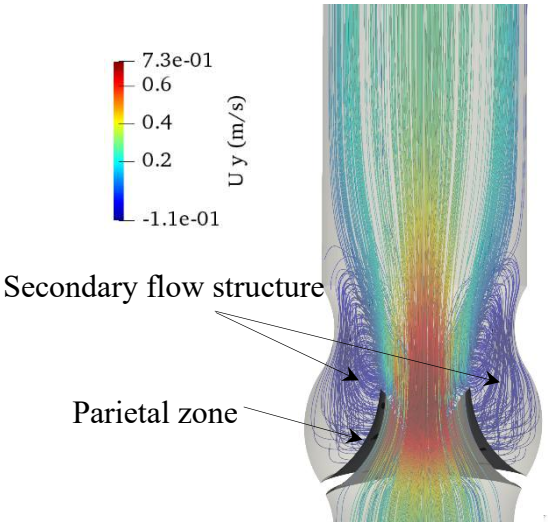
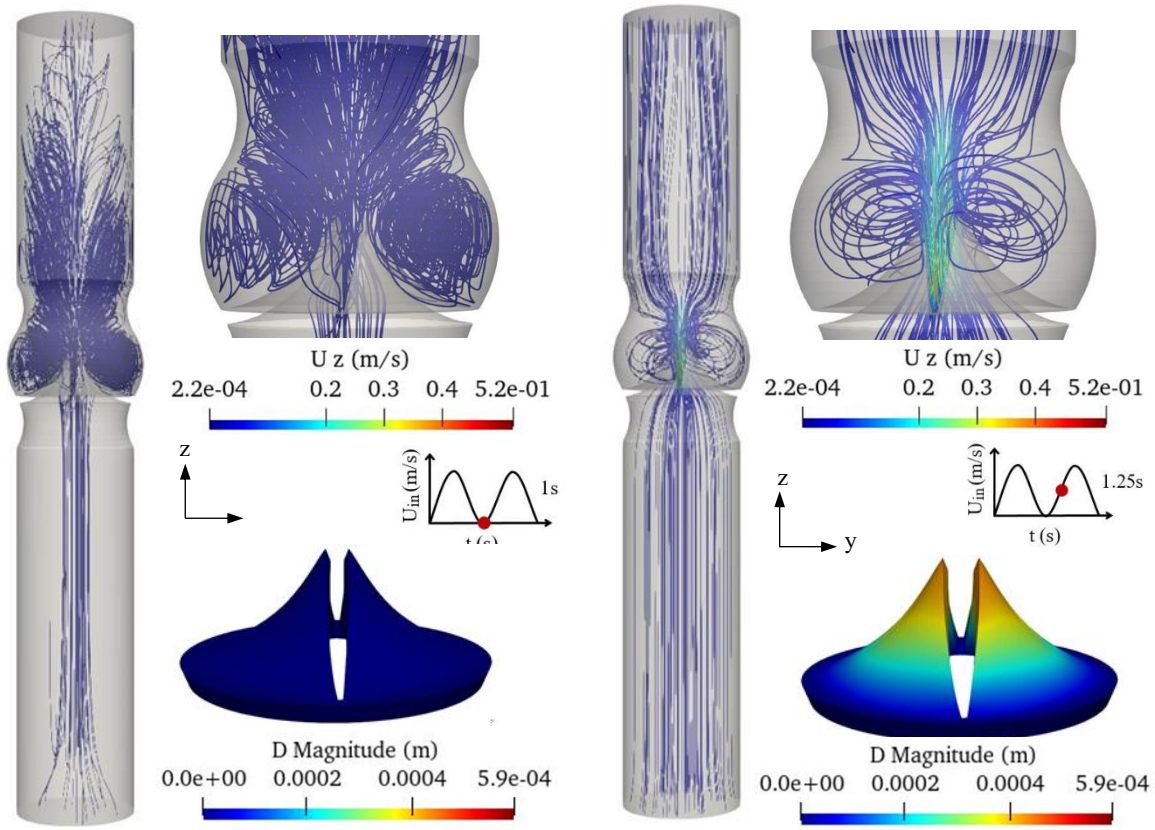
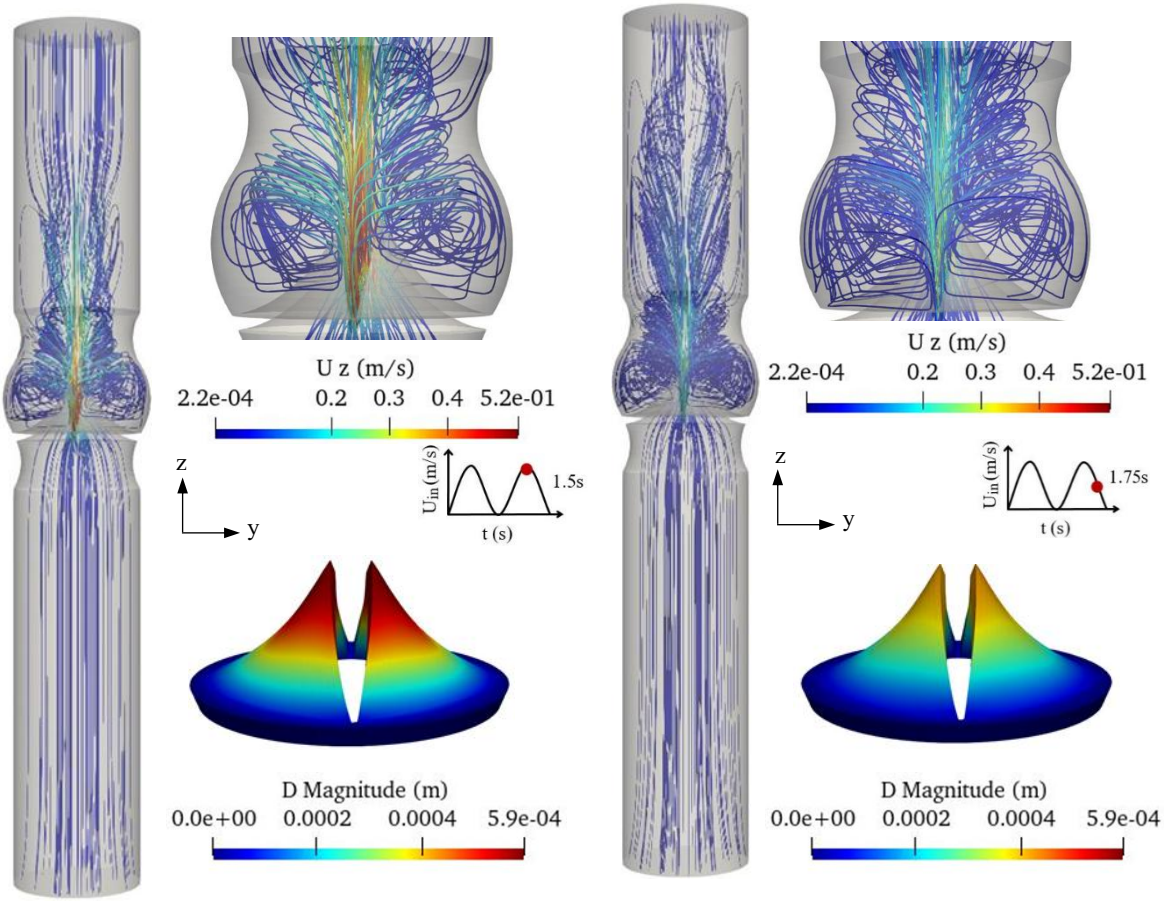


Figure 18. Streamlines of the blood flow for wide span valve opening with 0.2 m/s inflow velocity.

Uniform blood flow passing through the valve opening gets its maximum high, two vortexes start falling backward and push the separated valve leaflets downside (see Figure 18). This mostly closed circulatory flow field can be the major cause for keeping down the blood pool continuously, and consequently increasing the risk of thrombose formation. The main part of blood is being carried away through the high-velocity zone only small fraction of the blood enters to the secondary back flow region most located near to wall and parietal zone. In the following sections, wall shear stress (WSS) based indexes are used for further analysis of the thrombose formation and stasis conditions at venous valve region.


U z (m/s)
2.2e-04 0.2 0.3 0.4 5.2e-01
z
U_{in} (m/s)
1s
t (s)
D Magnitude (m)
0.0e+00 0.0002 0.0004 5.9e-04
U z (m/s)
2.2e-04 0.2 0.3 0.4 5.2e-01
z
y
U_{in} (m/s)
1.25s
t (s)
D Magnitude (m)
0.0e+00 0.0002 0.0004 5.9e-04


U z (m/s)
2.2e-04 0.2 0.3 0.4 5.2e-01
z
y
U_{in} (m/s)
1.5s
t (s)
D Magnitude (m)
0.0e+00 0.0002 0.0004 5.9e-04
U z (m/s)
2.2e-04 0.2 0.3 0.4 5.2e-01
z
y
U_{in} (m/s)
1.75s
t (s)
D Magnitude (m)
0.0e+00 0.0002 0.0004 5.9e-04

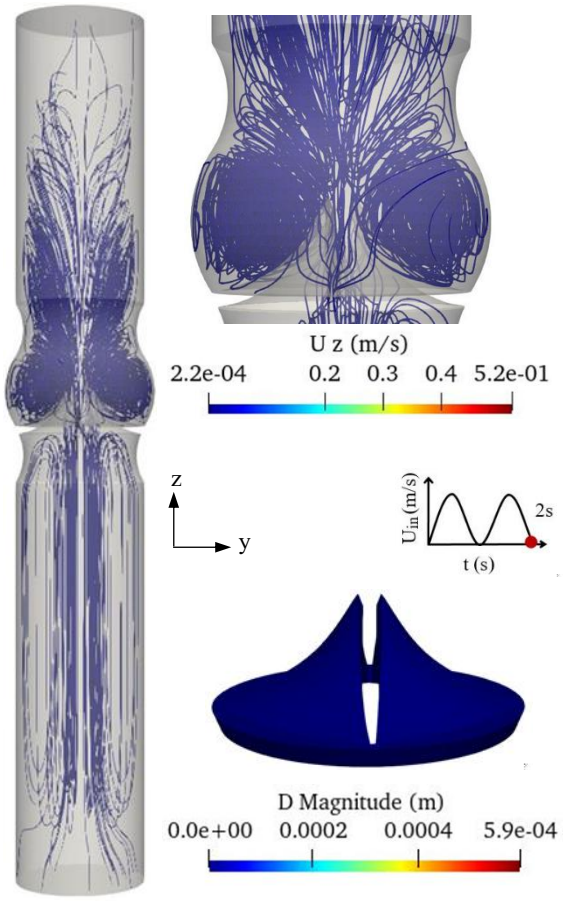
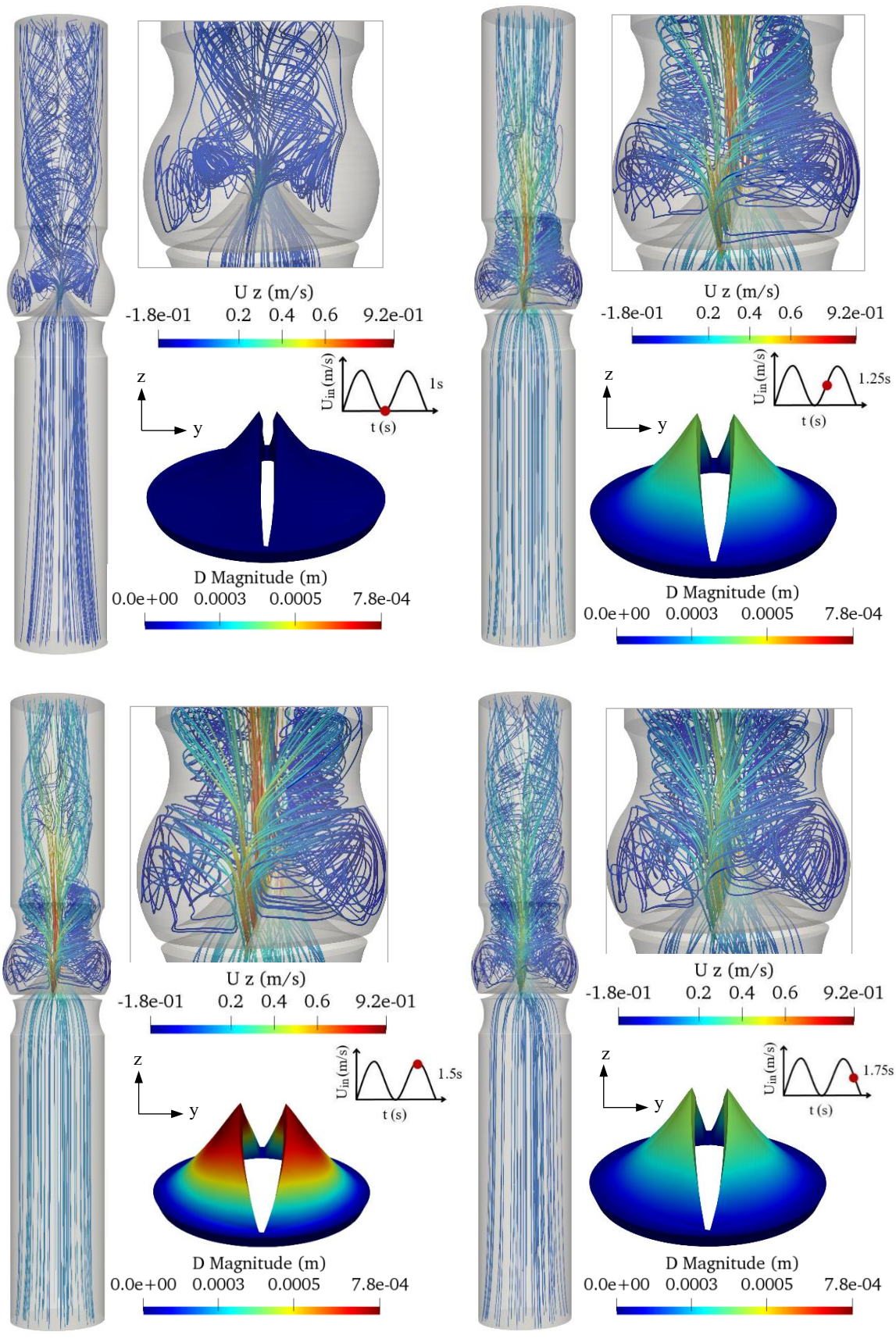


Figure 19. Streamline distributions of FSI model for five different instantaneous sinusoidal inlet velocities with maximum amplitude of 0.05 m/s.

Streamlines of blood flow and valve displacements in deep vein geometry are presented in Figures 19-21 for periodical sinusoidal inlet velocities with three magnitudes 0.05, 0.1 and 0.2 m/s. Maximum velocities and valve displacements are observed at the maximum velocity amplitudes as expected. Length of the secondary back flow separation zone is observed as proportional with the flow rate thus instantaneous changes occur during the varying blood flow. Blood flow at the back pockets of venous valve has almost closed loop circulation and its angular velocity increases with the increasing valve leaflets openings. Results show that, due to gravity and wall surface effects, secondary back flows occur above the valve and sinus region and its separation zone is varying as a function of blood velocity and valve leaflet displacements. At maximum velocity amplitudes shown in Figures 19-21, velocity streamlines move parallel to venous wall at 0.05 m/s. and start to generate whirling flow at higher velocities (0.1 and 0.2 m/s.) due to the effect of upper sinus geometry and leaflet induced flow. At the closing phase of the valve leaflets velocities drop as expected while blood column fills the upper sinus region due to the effect of secondary back flow and gravity. Whirling flow occurs and grows at the upper portion of deep vein starting from venous sinus region with the increasing blood flow. Main reason can be attributed to complex hemodynamic interaction of blood flow with both structural response of leaflet form and upper sinus region geometry. We assumed a uniform sinusoidal inflow blood flow for these simulations but it is observed that for higher velocities upper deep vein compartment having the same venous valve mechanism subjects to a whirling inflow blood flow. This cascading flow mechanism in deep vein deserves further detail analysis.


U z (m/s)
-1.8e-01 0.2 0.4 0.6 9.2e-01
z
y
U_{in} (m/s)
t (s)
1s
D Magnitude (m)
0.0e+00 0.0003 0.0005 7.8e-04
U z (m/s)
-1.8e-01 0.2 0.4 0.6 9.2e-01
z
y
U_{in} (m/s)
t (s)
1.25s
D Magnitude (m)
0.0e+00 0.0003 0.0005 7.8e-04
U z (m/s)
-1.8e-01 0.2 0.4 0.6 9.2e-01
z
y
U_{in} (m/s)
t (s)
1.5s
D Magnitude (m)
0.0e+00 0.0003 0.0005 7.8e-04
U z (m/s)
-1.8e-01 0.2 0.4 0.6 9.2e-01
z
y
U_{in} (m/s)
t (s)
1.75s
D Magnitude (m)
0.0e+00 0.0003 0.0005 7.8e-04

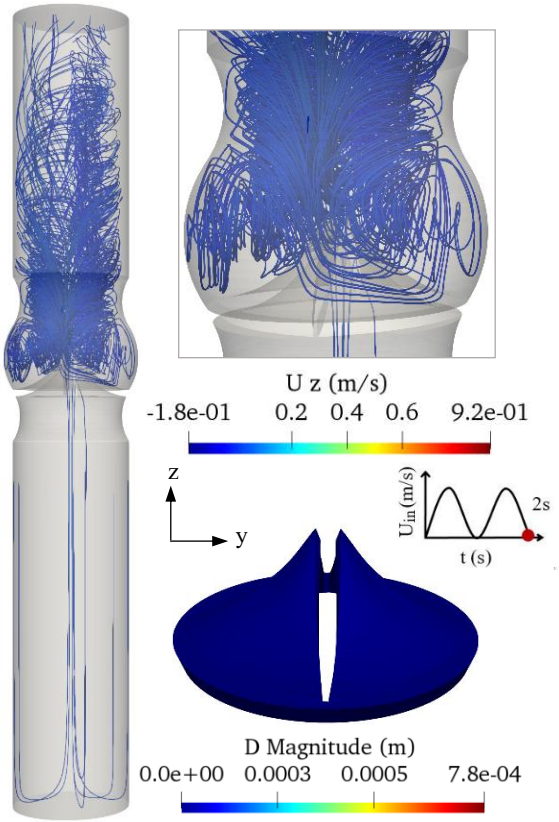
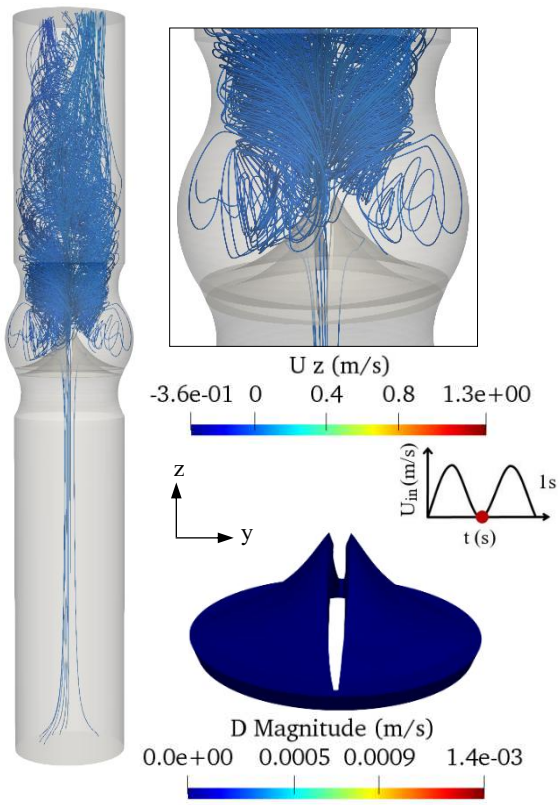
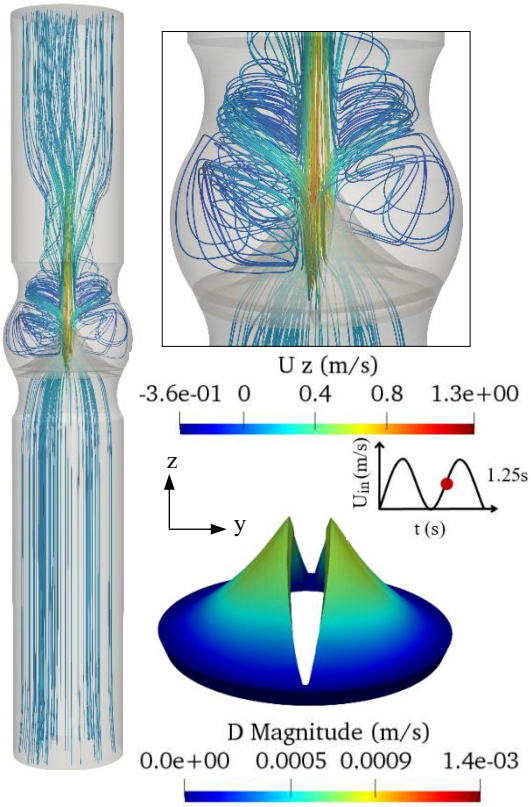


Figure 20. Streamline distributions of FSI Model for five different instantaneous sinusoidal inlet velocities with maximum amplitude of 0.1 m/s.





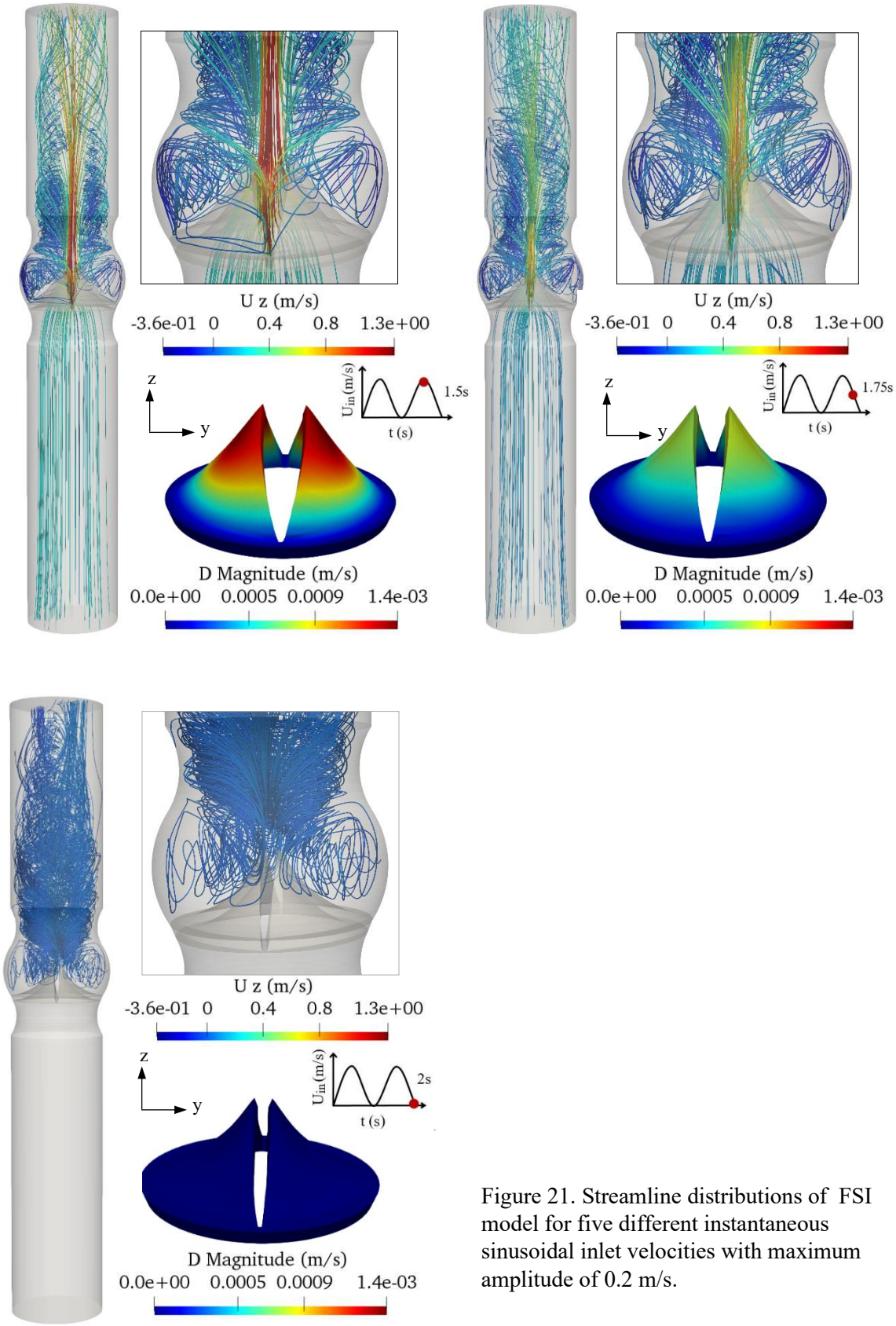


Figure 21. Streamline distributions of FSI model for five different instantaneous sinusoidal inlet velocities with maximum amplitude of 0.2 m/s.

Vascular compliance and venous return: Diameter change in venous valve sinus region results in transferring less blood volume during the narrow valve opening. Pressure wave reflection resulting from critical diameter chance in sinus exit can force venous compliance to adopt itself to prevent excessive increases in blood pressure. Decreased venous compliance is one of the transient changes in venous return. Normally, sympathetic vein activation reduces venous compliance, increases central venous pressure and thus promotes venous return. Gravity also plays an important role on venous return when a person stands up (vertical vein as in our case). In this case, paradoxically pressure gradient for venous return increases but venous return on the contrary decreases. The main reason can be attributed to falling right atrial pressure and ventricular preload, and stroke volume decreased by the Frank-Starling mechanism.

Vascular compliance is the ability of a vein wall to expand and contract passively with the internal pressure changes. This feature allows to distend and increase volume with increasing transmural pressure and it is quantified as vessel compliance $C = \Delta V/\Delta P$ which is the fraction of change in volume to pressure. In Figure 22, two critical features stand out. One is slope at a given pressure is different and the second is the compliance of a vein is about 10-20 times greater than an artery at lower pressure (< 15 mmHg). As a result of this veins can handle large displacements in blood volume with a small change in pressure. As extreme cases where the pressure is less than 10 mmHg, vein collapse may occur. In deep vein case, under harmonic sinusoidal inflow oscillations, we frequently observe less blood volume and low internal pressure at low velocities. Figure 22 shows that when the flow velocity increases four times, relative volume and compliance increase 50% percentage which gives high adaptivity to flow resistance. It can be concluded that, for the same pressure, low blood resistance leads to a higher flow rate and venous return.

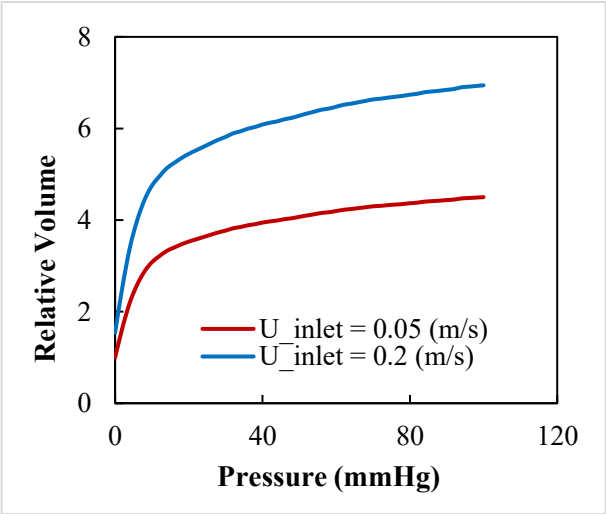
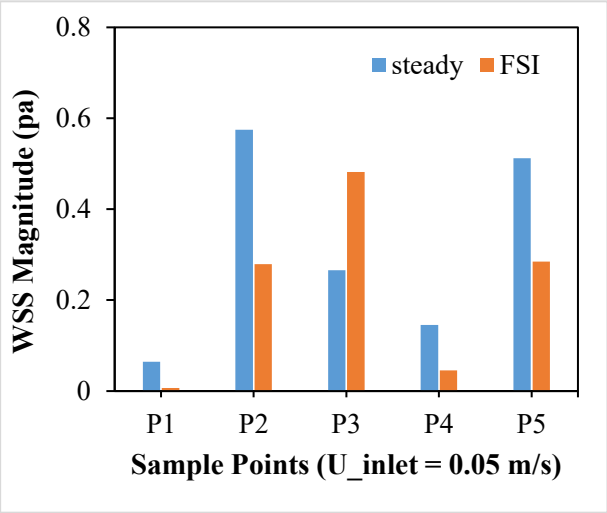


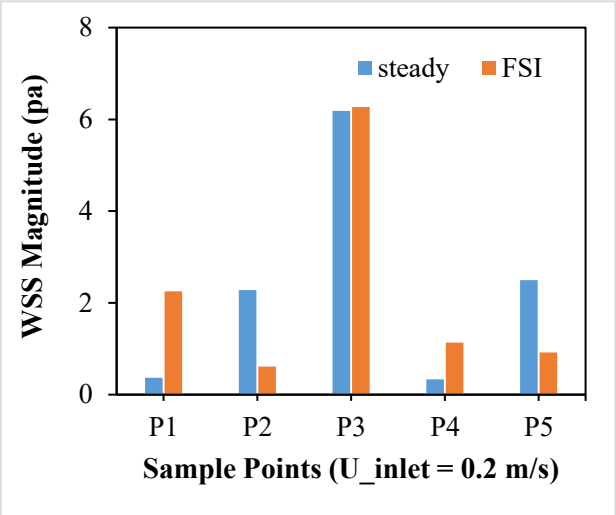
Figure 22. Deep vein compliance for slow and high blood flow.

4.1.4 Temporal Variations of WSS

Temporal variations of WSS are studied at some critical points of deep vein and venous sinus throughout the single harmonic (sinusoidal) cycle as shown in Figure 23. Comparisons of rigid wall and FSI models for specific valve openings demonstrated at five locations (between P1 and P5) for low (0.05 m/s) and high (0.2 m/s) blood velocities. Results show that temporal WSS distribution along the deep vein and venous sinus varies essentially in the presence of pulsatile flow due to considerably affected blood hemodynamics. FSI model captures this harmonically changing velocities and WSS distributions. For lower blood velocity, steady results estimate higher WSS magnitudes compared to FSI case except at point P3 where higher reverse secondary flow observed. For higher blood velocity, WSS magnitudes increase significantly and maximum WSS's occur at point P3. Steady flow over estimates the stresses at point P2 independent from the value of velocity. Lowest WSS distribution occurs at the back pockets of the venous valves and this

finding supports the idea that stasis blood condition mostly tends to occurs at zone P2. But it is required to support this finding with the results of time residency and other critical hemodynamic index values which will be discussed in the following section.





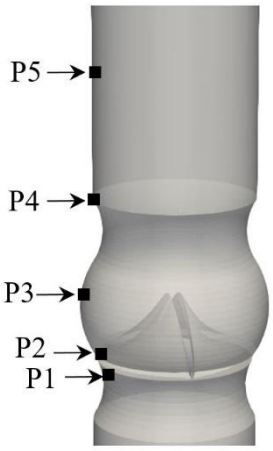


Figure 23. Temporal variations of WSS throughout the single harmonic cycle at various points on the wall (a) At P1, located at the lower left end of venous sinus, (b) At P2, located at the lower root of left valve, (c) At P3, located at the mid-point of left venous sinus, (d) At P4, located at the top corner of left venous sinus, (e) At P5, located at the left side of venous outlet.

4.1.5 Hemodynamic Index Analysis

Detecting the critical regions related to clot/thrombosis formation through stasis condition and shear thinning effects of the blood on the deep vein walls such as development of atherosclerosis brings out the importance of additional hemodynamic index study. WSS based index analysis is used for capturing the critical hemodynamic flow characteristics of blood mostly affected by velocity, flow geometry, viscosity and shear rate under isothermal flow condition. Hemodynamic flow anomalies in a deep vein geometry refer not only stasis formation at the back pockets of valve but also valve and venous wall dysfunctionalities. Following dimensionless index formulations capture hemodynamic blood flow anomalies and provide a concrete risk assessment for the conditions which may lead to a clot/thrombosis formation in deep veins.

4.1.5.1 Time Averaged Wall Shear Stress (TAWSS)

Instantaneous WSS vectors on the venous wall and valve leaflets throughout a single period is calculated by TAWSS. We focus both on high WSS values (greater that 10 - 15 N/m^2) for the possibility of

endothelial trauma, thrombosis formation, hemolysis and low values (lower than 0.4 N/m^2) for vessel wall and leaflet thickening and deformations.

Figures 24 - 25 and 26 - 27 show TAWSS distributions for wide and short-span valve openings using Casson and Bird-Carreau viscosity models. TAWSS is proportional to the wall shear stress (WSS) with the time averaging over a period, as the inlet velocity increases ($U_{inlet} > 0.05\ m/s$) so does the values of TAWSS, constantly. Results show that there are some pattern similarities between the index distributions of two viscosity models, however WSS magnitudes of Bird-Carreau model have higher estimates in general.

Considering the back view of the deep vein sinus walls (in Figures 24 and 26) where the accelerated up-sloping stream hits the back wall of valve leaflet edges simultaneously, higher values of TAWSS occurs. As mentioned before, high values of TAWSS (greater that 10 - 15 Pa) can cause endothelial trauma, thrombus and hemolysis. A resembling index pattern can also be observed around the valve`s tips (in Figures 25 & 27) as the flow gets accelerated where the area begins to shrink. Results indicate that venous valve leaflets and their cusps subject to highest WSS and TAWSS distributions during the valve opening.

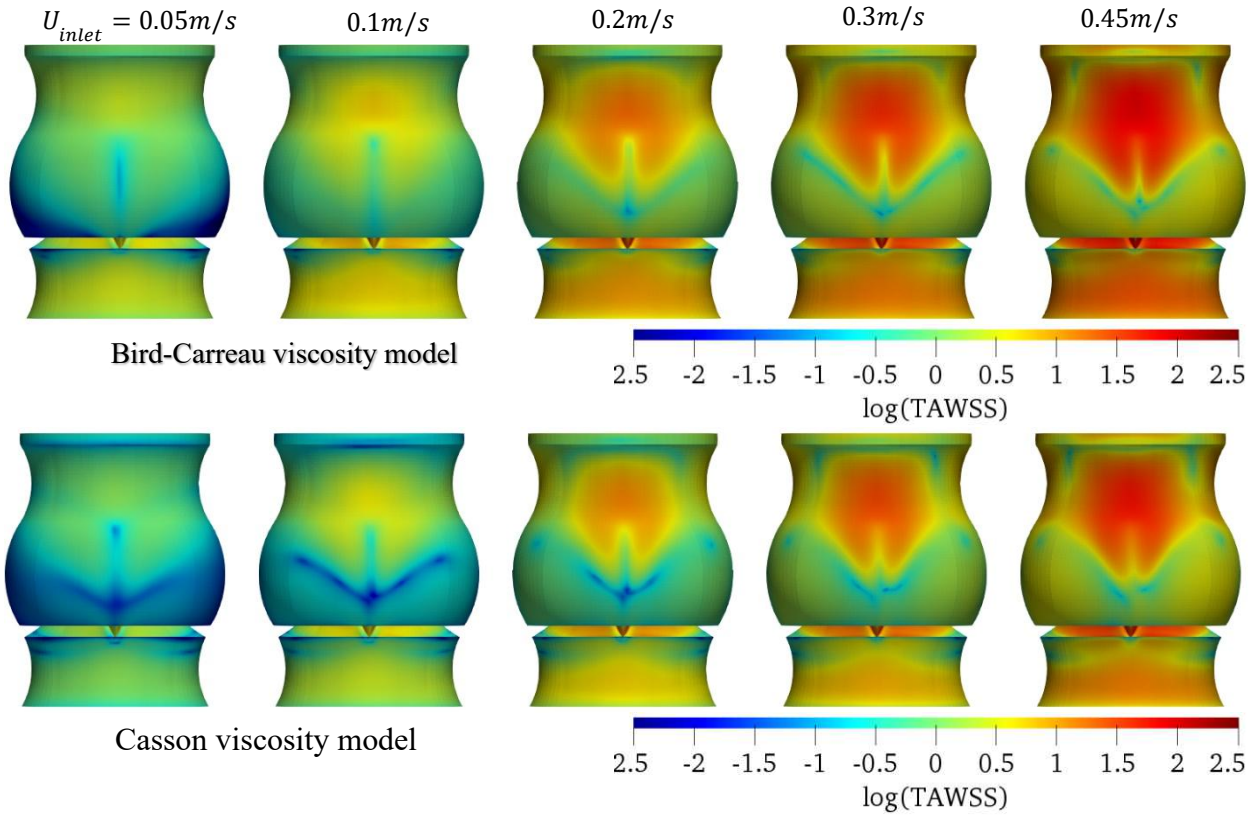


Figure 24. TAWSS distribution on the vessel wall for the wide-span venous valve opening.

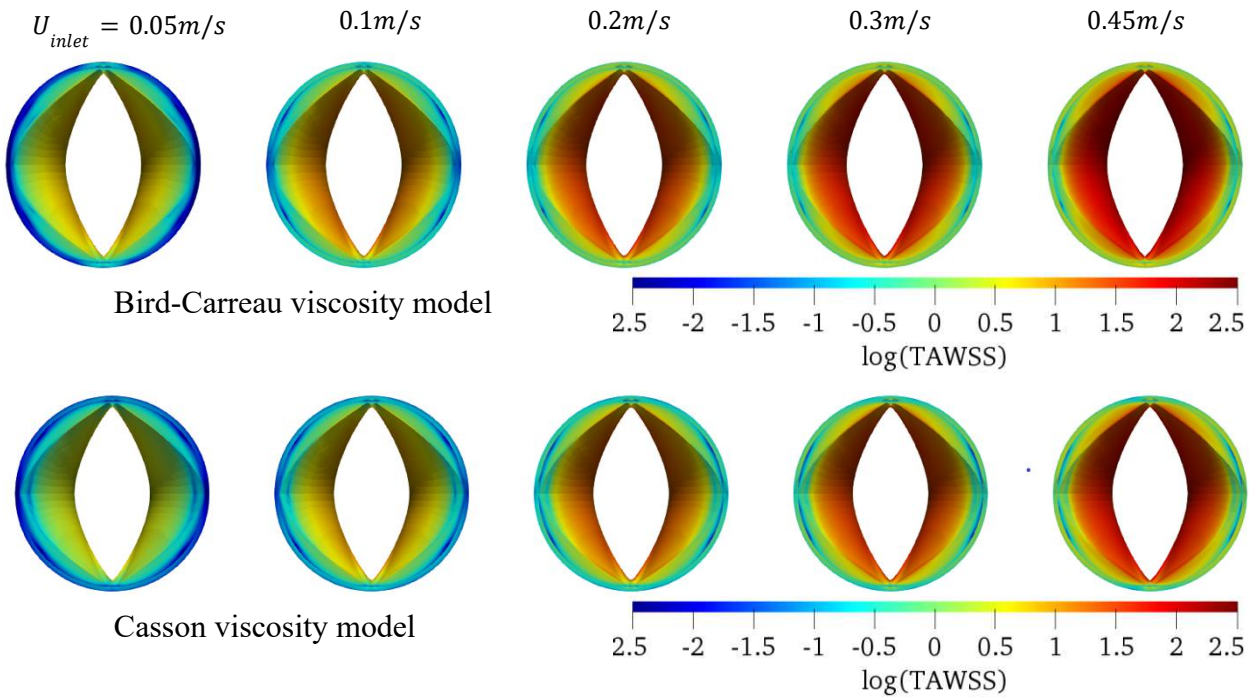


Figure 25. TAWSS distribution around the venous valve for wide-span opening.

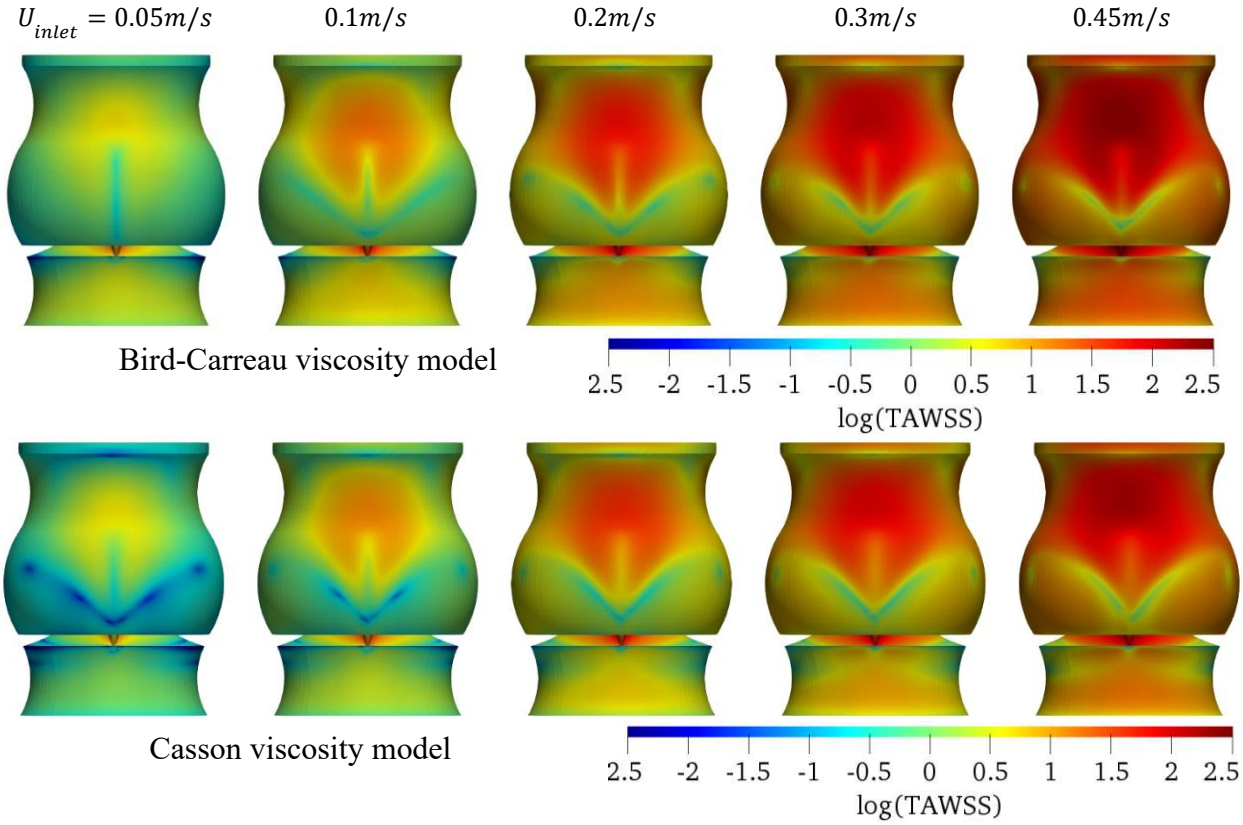


Figure 26. TAWSS distribution on the vessel wall for the short-span valve opening.

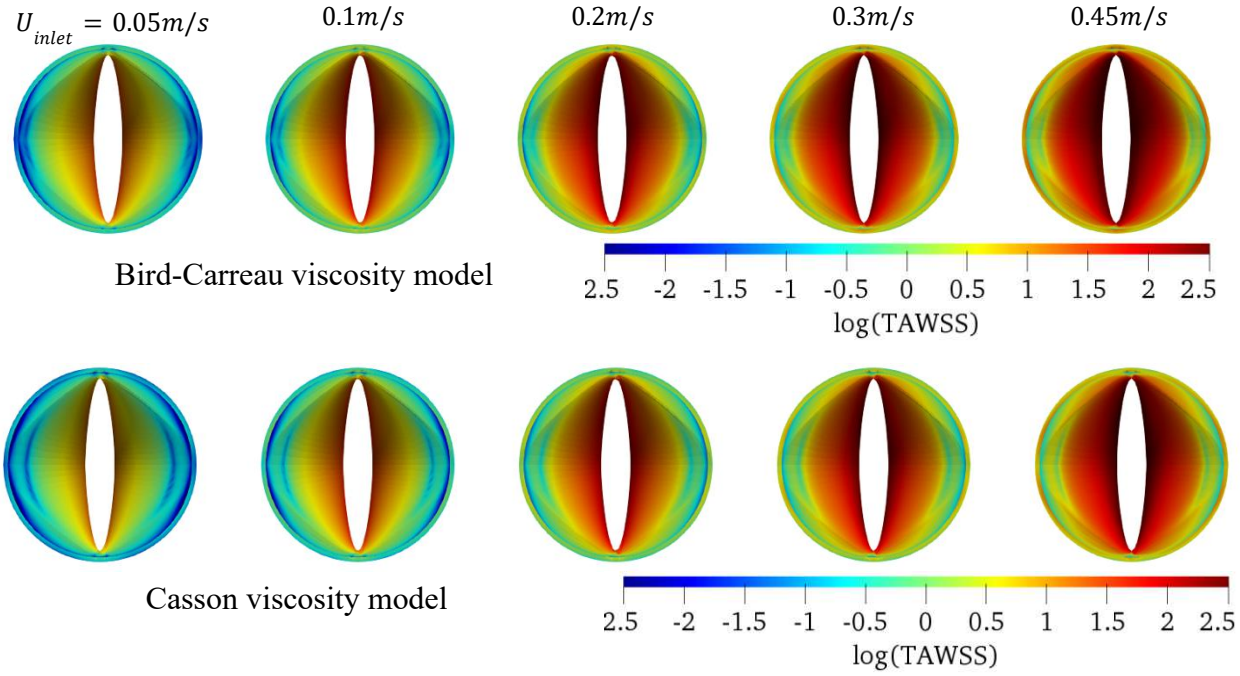
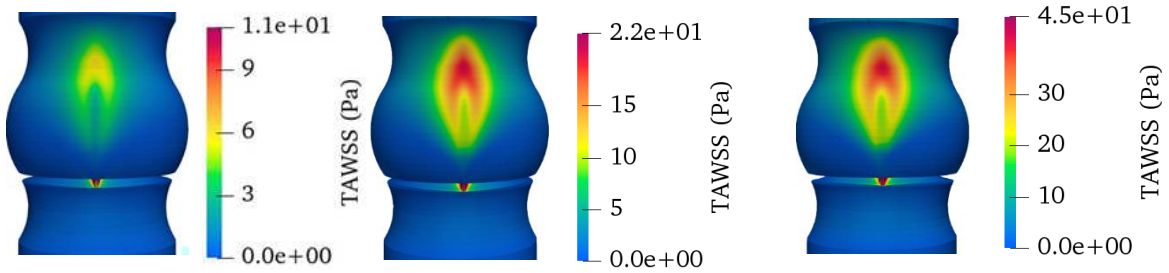
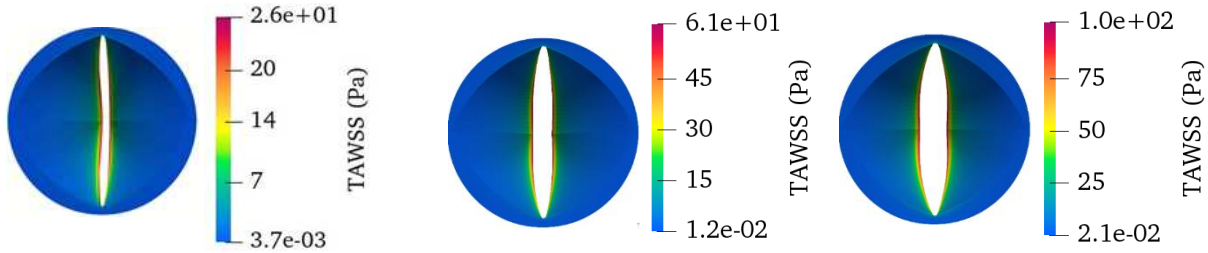


Figure 27. TAWSS distribution around the venous valve for short-span opening.



(a) U_{mag} = 0.05 m/s (b) U_{mag} = 0.1 m/s (c) U_{mag} = 0.2 m/s.

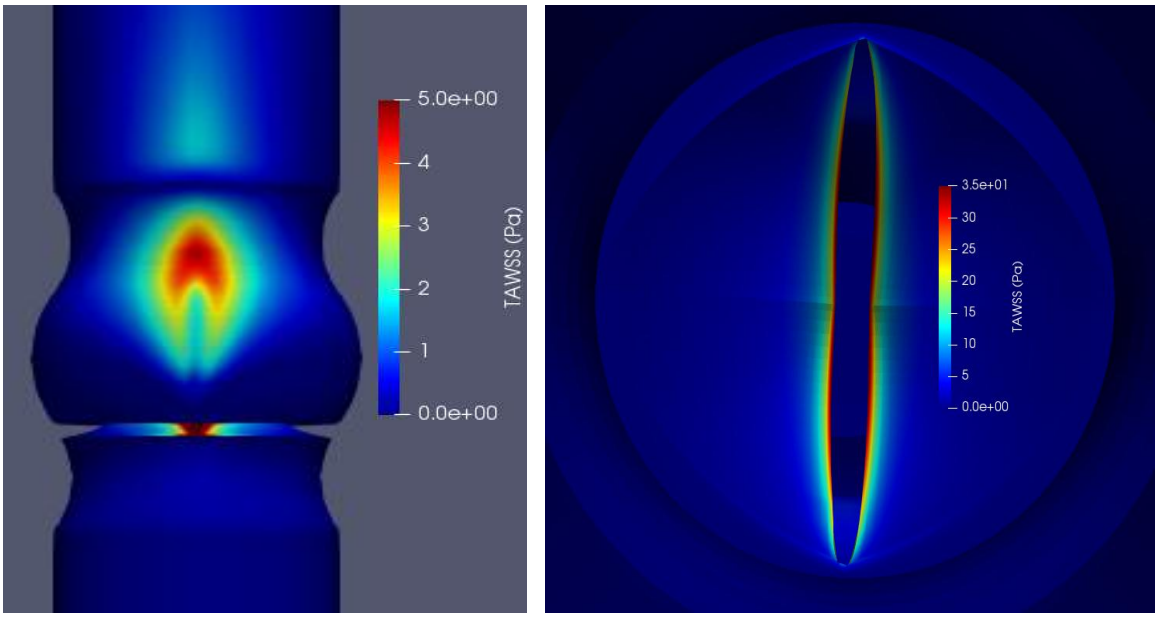
Figure 28. TAWSS distribution on the deep vein sinus wall.



(a) U_{mag} = 0.05 m/s (b) U_{mag} = 0.1 m/s (c) U_{mag} = 0.2 m/s.

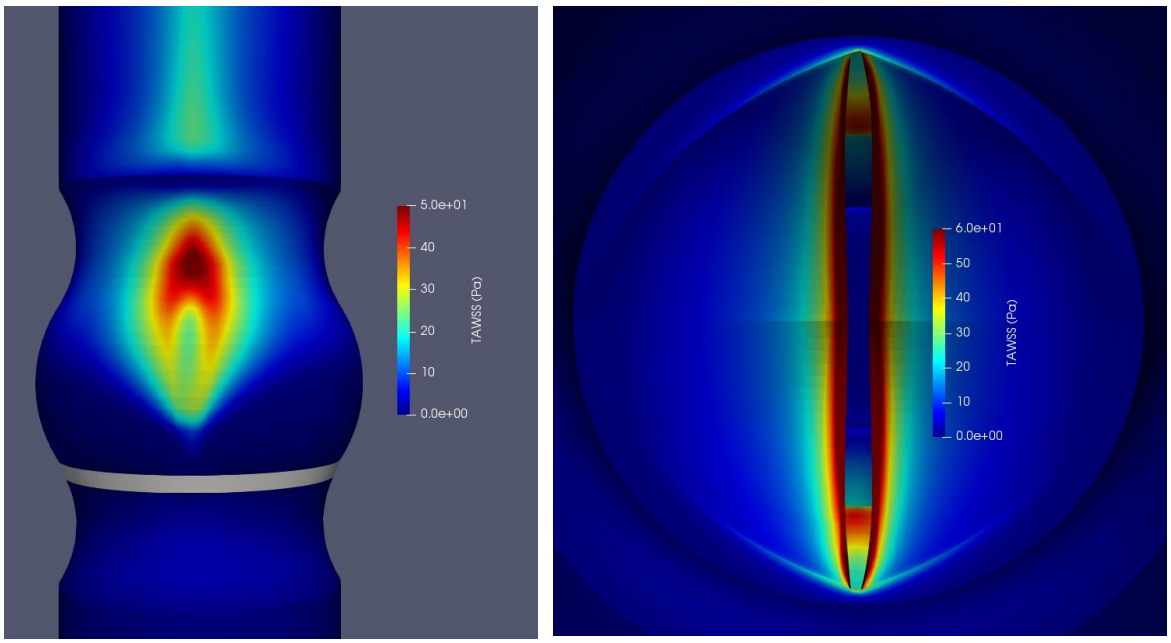
Figure 29. TAWSS distribution on the deep vein valve leaflets (top view) .

For the FSI model, TAWSS is calculated for low and high amplitude sinusoidal oscillating velocities (0.05 m/s and 0.2 m/s) as shown in Figures 30 and 31.



a) Deep vein sinus region b) Venous valve top view

Figure 30. TAWSS distributions of sinusoidal inflow velocity with amplitude 0.05 m/s.



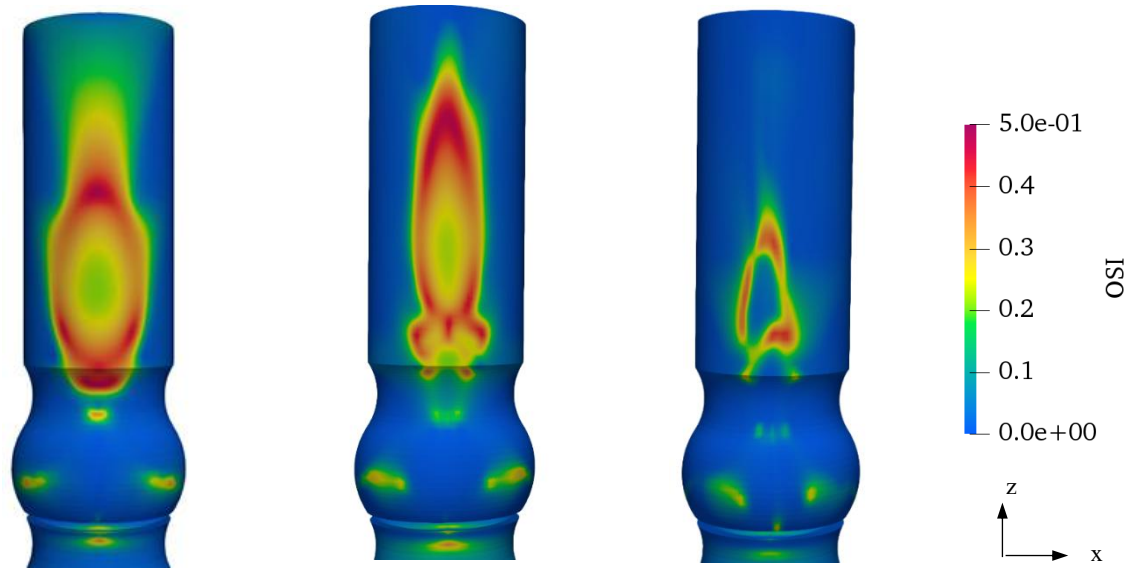
a) Deep vein sinus region b) Venous valve top view

Figure 31. TAWSS distributions of sinusoidal inflow velocity with amplitude 0.2 m/s.

Compared to sinus wall, valve leaflet cusps are subjected to significantly higher TAWSS values around 30 Pa and 60 Pa as seen in Figures 30b and 31b, respectively. This result obtained as the dimensionless number which is the average value of one period oscillating flow and shows much reliable results than fixed valve model focuses only a single instance of the valve opening. FSI results reveal that there is a risk of thrombosis formation at the tips of leaflets due to the higher TAWSS values. It should be noted that the risk of thrombosis formation may only be occur if these high TAWSS conditions persist continuously for a reasonable period of time. Further study is needed to investigate this period of time under different conditions and scenarios.

4.1.5.2 Oscillating Shear Index (OSI)

OSI is used for identifying the regions with high oscillating WSS values changing between 0 and 0.5. Index calculates high oscillatory WSS regions during one period of time. OSI distributions on deep vein geometry are obtained in Figure 32 as a function of changing inflow velocity.



(a) U_{inflow} = 0.05 m/s (b) U_{inflow} = 0.1 m/s (c) U_{inflow} = 0.2 m/s.

Figure 32. OSI distribution on deep vein sinus and its upper wall.

OSI index shows that high WSS oscillations are observed unexpectedly at low velocities rather than high velocities. WSS oscillations occur on the limited locations when the momentum effects become dominated in the flow region. However OSI index could not explain the magnitudes of WSS oscillations in these regions directly. But we learn this indirectly by hemodynamic observations that WSS magnitudes are usually low in the low velocity flow fields. It can be concluded that, for low blood velocities, WSS oscillations and their impact zones increase but their magnitudes relatively reduce. Additionally, we observe small oscillation zones on the sinus and right below to sinus region as shown in Figure 32, however their locations and oscillations change slightly with the increasing flow velocities.

Due to distal impedance in the circulation and the non-linear inertia of blood flow in deep vein and sinus region, a time lag arises between the oscillating WSS and circumferential stress (CS). This phase lag is characterized by the temporal phase angle between CS and WSS and called the "Stress Phase Angle" (SPA). Especially in the secondary reverse flow region, changes in SPA may have significant effects on gene expression but researches indicate that OSI has larger effects than SPA for many genes. Our findings in the secondary back flow region show that OSI gets values 0.4 and bigger. This means consistent and long-term oscillations of WSS in the secondary back flow may have a significant impact on venous wall.

4.1.5.3 Relative Residence Time (RRT)

Relative residence time (RRT) is another major hemodynamic parameter that is closely bound up with long term presence of blood in a particular space, and consequently, is a good indicator for the thrombosis formation phenomena. Following Figures 33 - 34 and 35 - 36 illustrate the RRT distributions for wide and short-span valve openings using Casson and Bird-Carreau viscosity models under uniform steady flow. RRT uses TAWSS and OSI indexes and indicates the risk of venous stasis (or venostasis) formation which is one of the three factors of virchow's triad.

Results, in general, show some pattern similarities between the index distributions of two viscosity models in higher blood inflow velocities, however there are some critical differences between two model predictions for lower velocities. The most important output of RRT calculations is that the conjunction regions (namely back pockets of a valve) where the vessel walls and valve leaflets have come together shows the most critical level for RRT especially if the inlet velocity is very low ($U_{inlet} < 0.1\ m/s$). Comparing the wide and short-span RRT results for the lower velocities $U_{inlet} \leq 0.1\ m/s$, RRT distributions in wide-span opening in Figures 33 and 34 are significantly higher than the short-span opening in Figures 35 and 36. But these results are still not reflecting the whole picture and for more reliable results full range of valve openings in one period of blood flow is needed.

Figure 37 illustrates RRT distributions of FSI model on deep vein geometry for three different sinusoidal blood velocities. Results show that, with the decreasing blood velocity, RRT values are increased and concentrated on some locations. Prominent concentration regions are the entrance of sinus, exit of sinus and upper sinus regions appear as the symmetric dual form on the deep vein walls. It is observed, for velocity 0.05 m/s, that maximum values of RRT are concentrated on three regions and reached to values around 100. Two of these three regions are the upper-zone where the turning point of secondary back flow starts and mid-zone where the secondary back flow mixes with the main flow mainly disturbed by valve leaflets. These two regions slightly change their vertical positions with the magnitude of inflow velocity. Relatively small third region is located at the entrance of the sinus corresponds to the root of symmetric opening edges of valve leaflets. Its position remains almost constant but RRT increase at low velocity as expected. Naturally, these results are quite different than the steady fixed valve opening cases. Maximum RRT values at velocity 0.05 m/s were observed around 2,5 and their locations were concentrated at back pocket regions with larger sizes. Similarly we observed roughly 150 percent (150%) differences in RRT results for higher blood velocities passing the wide-span valve opening. These differences were expected due to the fixed valve opening and uniform flow, and consequently not reflecting the actual hemodynamic flow characteristics as a whole.

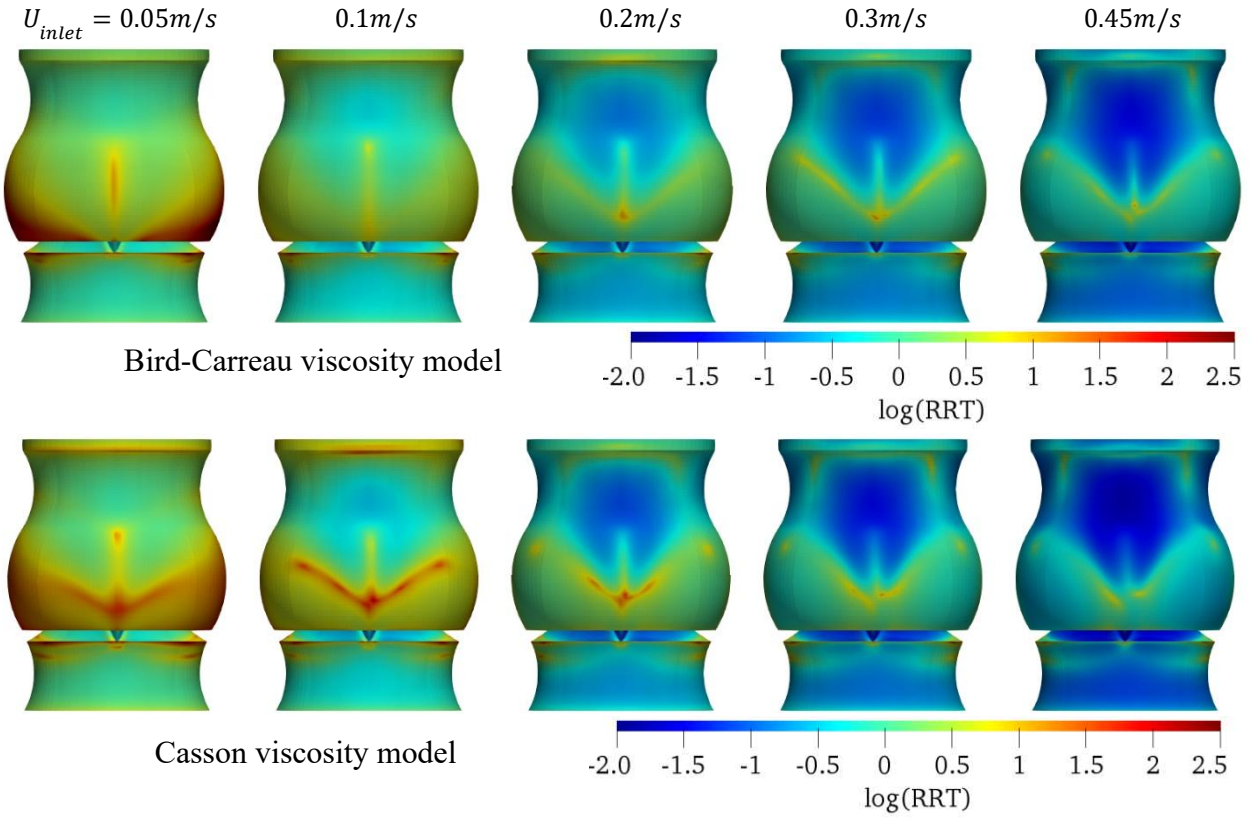


Figure 33. RRT distribution on the vessel wall for the wide-span valve opening.

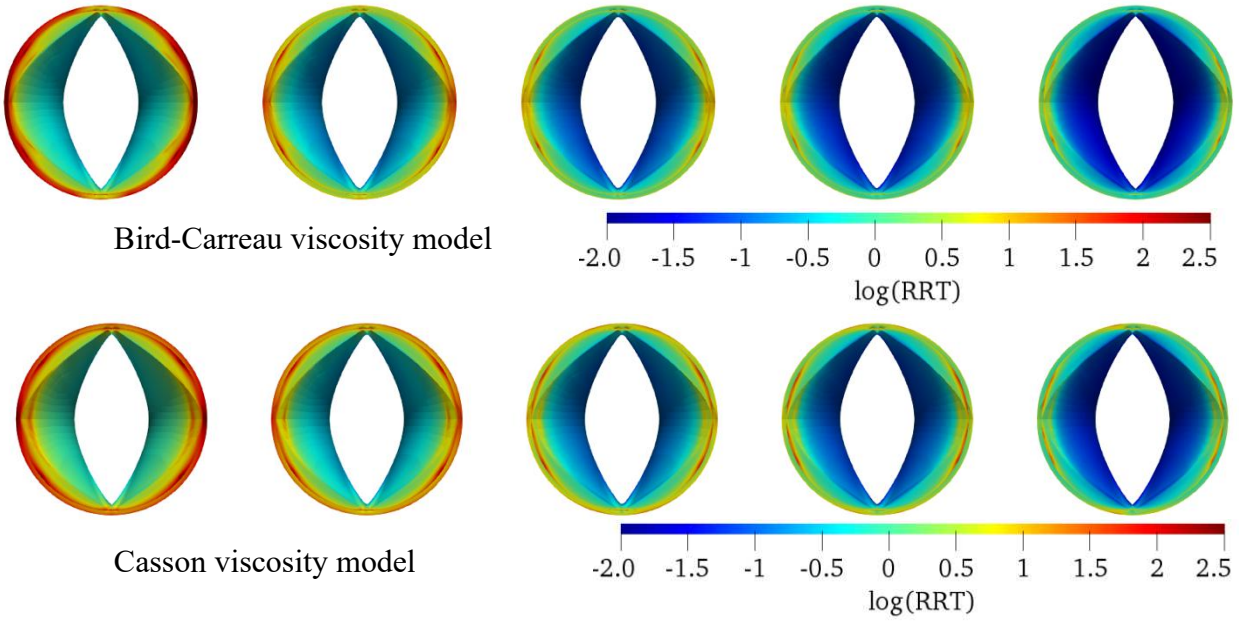


Figure 34. RRT distribution around venous valve for wide-span opening.

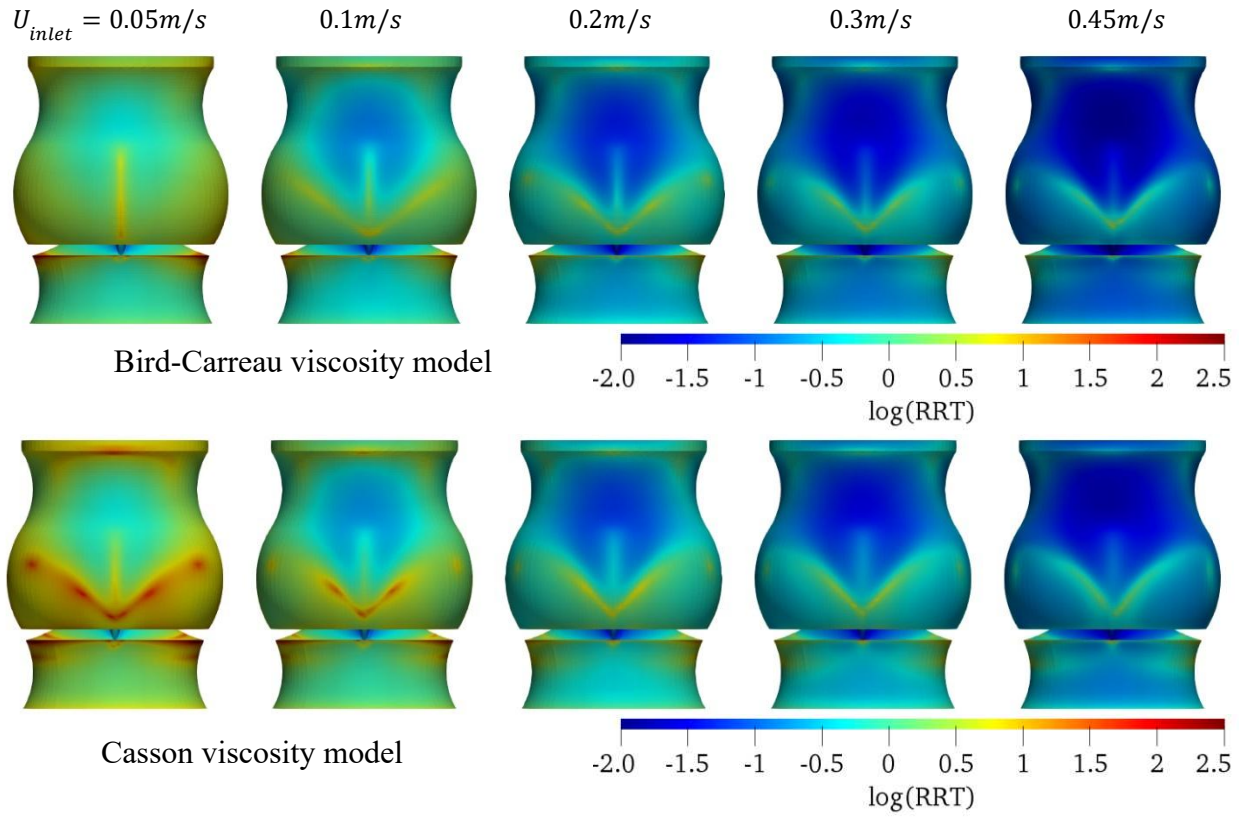


Figure 35. RRT distribution on the vessel wall for the short-span valve opening.

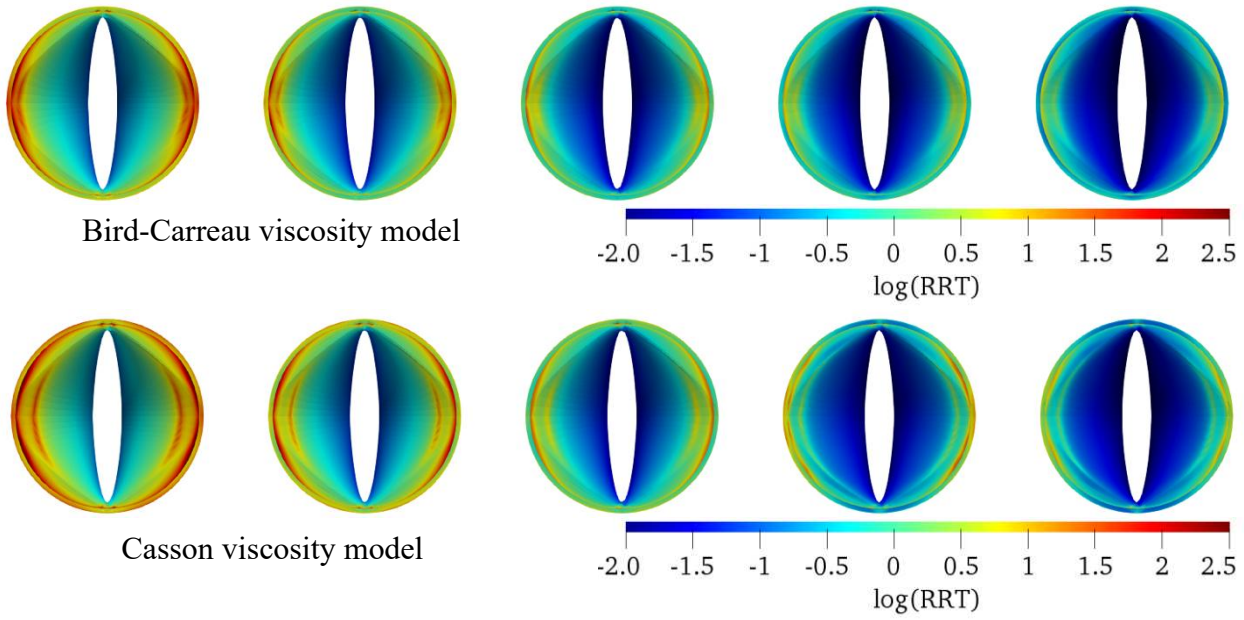
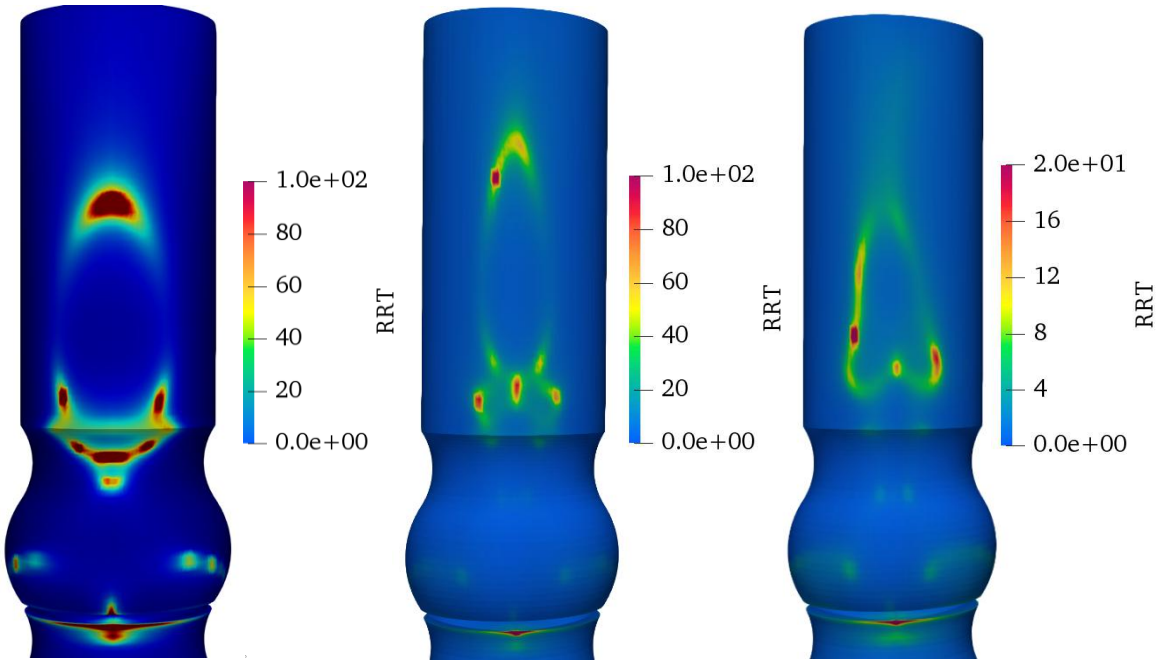


Figure 36. RRT distribution around venous valve for short-span opening.



(a) U_{inflow} = 0.05 m/s (b) U_{inflow} = 0.1 m/s (c) U_{inflow} = 0.2 m/s.

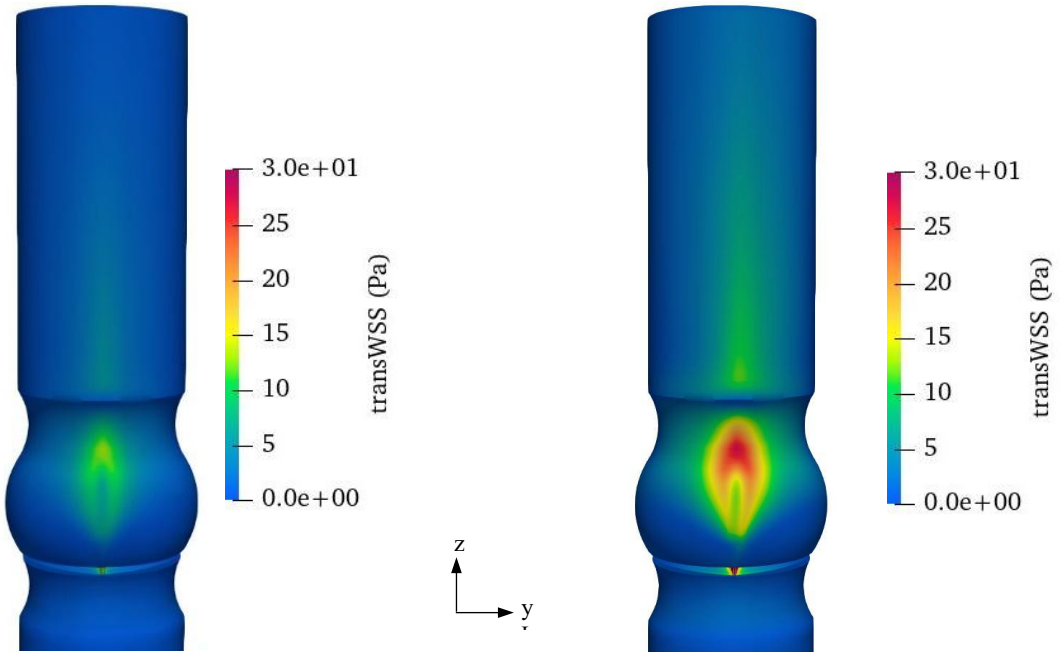
Figure 37. RRT distributions on the deep vein sinus and upper wall.

For the formation of thrombosis in deep veins and specifically in venous sinus region, regions having high OSI and high RRT values simultaneously play critical role and generate potential high risk for DVT. It is known in the literature (Jimenez and Davies, 2009) that both high OSI and RRT together stimulate to a platelet aggregation and their adhesion process and then lead to a thrombosis formation. On the other hand low OSI and high RRT regions are a good candidate for thrombosis as a result of longer residence time of micro particles in the stasis formation stage. From Figures 32 and 37, we observe similar concentration regions indicating high risks locations for thrombosis formation.

4.1.5.4 Transverse Wall Shear Stress (transWSS)

Capturing the multi-directional hemodynamic flow characteristics is a key factor for WSS distributions in deep vein simulations. This critical information may only be calculated by transWSS index under transient flow conditions. Low transWSS represents the existence of a parallel flow in a dominant flow direction. Index is independent from whether flow is uniform or pulsatile and similarly flow direction is whether forward or reversal. Figure 38 illustrates the transWSS distributions on the deep vein sinus and upper wall region. Results show that transWSS values increase with the increasing blood inflow velocity. High transWSS values mostly refer to: i) large disturbances in the main flow direction, ii) smaller disturbances in the main flow direction but they are effective in most part of the cardiac cycle (one period), iii) small disturbances in the direction of blood flow near to venous wall. The values of transWSS change between 0 and TAWSS.

In our case, high transWSS regions in sinus mostly results from large disturbances in the main flow direction, but we observe small disturbances in the opposite direction of the blood flow near to venous wall resulting from secondary back flow mostly occurs upper sinus region. On the other hand, smaller disturbances in the main flow direction are detected at the entrance of the sinus region generally effective in most part of the cardiac cycle.



(a) U_{inflow} = 0.1 m/s (b) U_{inflow} = 0.2 m/s.

Figure 38. transWSS distributions on deep vein sinus.

We know from the earlier works (David De Wilde, 2015) that the presence of both low TAWSS and low transWSS at the same location with the existence of high RRT values refers to a stationary blood pool which may potentially lead to a stasis condition. Studies that analyzed the non-trauma-related venous thrombi by autopsy and phlebography concluded that they originated in the valves and sinuses of the calf veins (Bovill and Vliet, 2011). It is reported in the literature that the most common site for initiation of the thrombus appears to be the valve pocket sinus, due to its tendency to become hypoxic. Activation of endothelial cells by hypoxia or possibly inflammatory stimuli would lead to surface expression of adhesion receptors that facilitate the binding of circulating leukocytes and macrovesicles. This finding also supported by the experimental works of Hamer *et al.* arguing that experimental stasis has been shown to result in a significant decline in oxygen tension in the venous back pocket sinus.

In the light of this criteria the most critical region for deep vein thrombosis (DVT) is the symmetric back pockets of venous valve (parietal zones) which may generate suitable conditions for blood stasis. Statistical results by Liu *et al.* show that, interestingly the number of valves in individuals can vary, and those with more valves have a higher frequency of DVT. Considering both clinical observations and our hemodynamic index analysis, symmetric back pockets in sinus have a critical importance for thrombosis formation.

5. Quantitative Assessment with Patient Data

In order to relate the slow/stagnant flow and venous stasis in deep veins to the risk of DVT occurrence in lower extremity, the findings of two clinical studies (Jensen *et al.*., 2017) and (Ashrani *et al*., 2009) are used for quantitative assessment. Both studies evaluated the underlying mechanisms for venous stasis syndrome and the correlation of slow venous flow with the subsequent DVT formation.

They found that DVT occurrence in patients with slow venous flow (21/482, 4.36%) doubled compared to the normal flow group (11/493, 2.23%). It is observed that there is no significant difference in peak velocities of oncology patients with or without DVT. DVT-related venous statis mechanism has a close correlation with venous valvular incompetence and venous outflow obstruction. On the other hand, DVT recurrence has a close association (6.4- to 9.6- fold increased risk) with venous stasis syndrome and its risk factor persists up to 20 years. These are statistical quantitative data observed in 297 patients (Ashari *et. al*.) and 975 patients (Jensen *et. al*.) in terms of percentage linking to DVT occurrence. We can justify from these quantitative data that slow venous flow and stasis syndrome increase the DVT risk and has a correlation with valvular incompetence mostly observed in valve root and outflow obstruction behind the valve and its vicinity.

Bark *et al.* studied thrombosis growth in an in-vitro experiment under the high pathological shear rates. They observed the platelet accumulation of whole porcine blood near occlusion in stenosis through image analysis of light microscopy. They found that thrombus accumulates four times faster at very high wall shear rates (1,000 – 30,000 s^{-1}) than normal physiological wall shear rates (<400 s^{-1}). The lag time, which is the duration from the starting of flow up to the first thrombus formation exceeded 10 μm in thickness, is increased with the reducing shear rates. Since this experiment is conducted in the collagen-coated stenosis under limited heparin add, findings support high shear rate-based thrombus formation theory. However, our results are mostly obtained under low shear rate flow and not much correlated with Bark *et.al.* except both high TAWSS and high transWSS locations mostly appears at the cusps of valve leaflets.

Quriel *et al.* introduced a volumetric index for the quantification of deep venous thrombosis to avoid some of the drawbacks of existing indices (Marder score, SVS/ISCV, Registry index) such as lack of clinical relevance, poor estimation of thrombus mass, and lack of important venous segments (Quriel et. al., 1999). Their venous volumetric index (VVI) is calculated with the combination of 14 actual venous segment volumes and normalized with the volumes of a single calf vein. They studied with the 885 patients with DVT and the results are compared with three existing methods for quantifying the venous thrombus burden. VVI and other existing indexes are mostly obtained by calculation of the data received from medical imaging devices and used for scoring of patients suffering from the DVT and related symptoms. Our approach, on the other hand, is based on hemodynamic simulation and has an ability of calculating precise WSS's interacting with the vessel and leaflet walls. Possible flow disorders and extreme conditions may reveal some indications of possible stasis conditions or thromboembolism with the help of hemodynamic indexes.

6. Discussion

Deep vein valve sinus is prone to thrombosis formation due to the irregular patterns of blood flow and the potential for a low oxygen tension. Modeling of the interaction between single-phase non-Newtonian blood flow and deformable venous valves using portioned FSI with strong coupling algorithms is very time consuming, one can easily conduct steady CFD analysis based on fixed valve assumption in order to evaluate the flow structure and hemodynamic indexes which would be beneficial for early-stage cardiovascular disease investigations. However, FSI would be beneficial in many ways. First, in comparison to the steady CFD analysis, FSI predicts the critical low flow field zones more precisely during venous return passive cardiac cycle or muscle contraction. The secondary back flow structures, for example, would combined together at the end of pumping cycle when the valve leaflets are in rested position. This phenomenon produces a highly viscous region right above the rested valve and back pockets of valve and increases the risk of thrombus formation. Second, the upcoming flow field widen the middle gap toward the side walls. Meanwhile the falling side flow fields bend the leaflets downside. Such displacement and deformation of valves destabilize the surrounding flow field and vice versa which emphasizes the importance of FSI consequently.

FSI results give more accurate and comprehensive results capturing the full period of flow hemodynamics, thus OSI and transWSS indexes are calculated which is not possible in steady simulations. It is observed that differences between index values of FSI and steady flow models are significant as expected.

7. Conclusion

The present numerical study points out several useful and rare subjects that gives us a real insight into the major factors of the thrombosis formation in deep veins using (i) steady CFD analysis of fixed-valve (ii) FSI analysis of unsteady blood flow and deformable venous valve. Some major findings of this comparative analyses are listed below:

i. Both Casson and Bird-Carreau shear thinning viscosity models produce reasonable results for the modeling of blood flow in deep vein despite the fact that Casson model seems to be more stable leading simulation to faster convergence.

ii. Steady hemodynamic analysis with a fixed valve assumption may benefit us to obtain faster practical solution of blood flow passing through the short and wide span valves, but FSI model captures the complex hemodynamics flow more comprehensively for the whole pumping cycle.

iii. Steady fixed and FSI hemodynamic models lead us toward the recognition of critical zones for venous thrombosis formation, but FSI (time depended coupled solution) model is absolutely more helpful due to the variation of critical zones through time and space.

iv. The irregular displacement and deformation of the valve leaflets destabilize the flow field, change the position and shape of secondary back flow fields.

v. FSI results indicate the risk of thrombosis formation at the cusps of leaflets due to high TAWSS values caused by higher inlet velocities. But the risk of thrombosis formation may only occur if these high TAWSS conditions persist continuously for a reasonable period of time. This finding compatible with Berk *et al.* results stating thrombus accumulates four times faster at very high wall shear rates.

vi. For the formation of thrombosis in deep veins, regions with high OSI and high RRT values play critical role and generate a high risk. It is known in the literature that both high OSI and RRT together stimulate to a platelet aggregation and their adhesion process and then lead to a thrombosis formation.

vii. Low OSI and high RRT regions such as back pockets of deep venous valves are a good candidate for thrombosis formation as result of longer residence time of micro particles in the venostasis stage.

viii. Possibility of endothelial cell trauma increases due to the high TAWSS values achieved with increasing blood velocities starting from 0.1 m/s inlet velocity.

ix. Presence of low TAWSS and high RRT at the same location together with low transWSS refers to a stationary blood pool which may potentially leads to a venous stasis condition. Our results indicate that some critical regions with low TAWSS and low transWSS also have high RRT values. Based on these findings the most critical region for deep vein thrombosis (DVT) should be expected as symmetric back pockets of venous valves.

Whirling flow mostly occurs and grows at the upper portion of deep vein valve starting from venous sinus region with the increasing blood flow repeating for each deep vein compartment. This cascading flow mechanism in deep veins through compartments deserves further detail hemodynamic analysis.

Acknowledgement

This work is funded by the Scientific and Technological Research Council of Turkey (TUBITAK) as ARDEB 1001 project under the grand numbers 117M430 and 120M671.

Conflict of interest statement

Authors certify that they have no affiliations with or involvement in any organization or entity with any financial, or non-financial interest in the subject matter or materials discussed in this manuscript.

References

Amaya R., Cancel L.M. and Tarbell J.M., (2016). Interaction between the Stress Phase Angle (SPA) and the Oscillatory Shear Index (OSI) Affects Endothelial Cell Gene Expression. PloS ONE 11(11). doi: 10.1371/journal.pone.0166569.

Ashrani A. A., Marc D. Silverstein, Brian D. Lahr, Tanya M. Petterson, Kent R. Bailey, and John A. Heit. (2009). Incidence and cost burden of post-thrombotic syndrome, Vascular Med., 14(4): 339–349, doi: 10.1177/1358863X09104222.

Aribas E. and Celebi, M. S. (2020). A thermal based RBC Aggregation model for two-phase blood flow. Korea-Australia Rheology Journal, *32*(2), 121–136. doi: 10.1007/s13367020-0011-8.

Aziz N. S., İbrahim N., Hafizzatul N., Harun I. M., & Abdullah K. (2015). Computational Fluid Dynamics Simulation of Early Diagnosis of Deep Vein Thrombosis. ARPN Journal of Eng. and App. Sci., Vol.10, No 19.

Bark D. L., Para A. N. and Ku D. N. (2012). Correlation of thrombosis growth rate to pathological wall shear rate during platelet accumulation. Biotechnology and Bioengineering, 109(10), 2642–2650, doi: 10.1002/bit.24537.

Bird R. B., Armstrong R. C. and Hassager O. (1987). Dynamics of polymeric liquids,Volume 1: Fluid Mechanics (2nd ed.). John Wiley & Sons.

Bovill E.G. and van der Vliet A. (2011). Venous valvular stasis-associated hypoxia and thrombosis, Annular Review Physiology, 73:527–545.

Bungart H.J. and Schäfer M. (2006). Fluid-structure Interaction: Modelling, Simulation, Optimization. Springer.

Cardiff P., Karac A. and Peter De Jaeger. (2018). An open-source finite volume toolbox for solid mechanics and fluid-solid interaction simulations. arxiv:1808.10736.

Causin P., Gerbeau J. F. and Nobile F. (2005). Added-mass effect in the design of partitioned algorithms for fluid–structure problems. *Computer Methods in Applied Mechanics and Engineering*, *194*(42–44), 4506–4527. https://doi.org/10.1016/j.cma.2004.12.005.

David De Wilde. (2015). Wall Shear Stress Metrics and Their Relation to Atherosclerosis: an Experimental and Computational Study in Mice, PhD Thesis, Institute Biomedical Technology Biofluid, Ghent University.

Hamer JD, Malone PC, Silver IA. (1981). The PO2 in venous valve pockets: it's possible bearing on thrombogenesis. Br J Surg., 68(3):166–170.

Hirt C., Amsden A. and Cook J. (1974). An arbitrary Lagrangian-Eulerian computing method for all flow speeds. Journal of Computational Physics, 14(3), 227–253, doi: 10.1016/00219991 (74)90051-5.

Jensen C.T., Antoun Chahin, Veral D. Amin, Ahmed M. Khalaf, Khaled M. Elsayes, NicolausWagner Bartak, Bo Zhao, Shouhao Zhou, and Deepak G. Bedi. (2017). Qualitative Slow Blood Flow in Lower Extremity Deep Veins on Doppler Sonography, J Ultrasound Med Sep; 36(9): 1867–1874, doi: 10.1002/jum.14220.

Jimenez J.M. and F.P. Davies. (2009). Hemodynamically driven stent strut design, Ann Biomed Eng., 37:1483–94.

Jung J. M., Lee D. H., Kim K. T., Choi M. S., Cho Y. G., Lee H. S., Choi S. I., Lee S. R., and Kim D. S. (2014). Reference intervals for whole blood viscosity using the analytical performance evaluated scanning capillary tube viscometer. Clinical Biochemistry, 47(6), 489–493. doi:10. 1016/j.clinbiochem.2014.01.021.

Küttler U. and Wall W. A. (2008). Fixed-point fluid–structure interaction solvers with dynamic relaxation. Computational Mechanics, 43(1), 61–72. https://doi.org/10.1007/s00466-008-0255-5.

Kyrle P. A. and Eichinger S. (2005). Deep vein thrombosis. The Lancet, *365*(9465), 1163–1174. doi: 10.1016/S0140-6736(05)71880-8.

Liu G.C., Ferris EJ, Reifsteck JR, Baker ME. (1986). Effect of anatomic variations on deep venous thrombosis of the lower extremity. Am. J. Roentgenol., 146(4):845–848.

Lonyai A., A. M. Dubin, J. A. Feinstein, C. A. Taylor, and S. C. Shadden. (2010). New insights into pacemaker lead-induced venous occlusion: simulation-based investigation of alterations in venous biomechanics. Cardiovasc. Eng. 10:84–90.

Matthies H. G. and Steindorf J. (2003). Partitioned strong coupling algorithms for fluid–structure interaction. Computers & Structures, 81(8–11), 805–812. doi: 10.1016/S00457949(02)00409-1.

Mazumdar J.N. (2004). BioFluid Mechanics, World Scientific, ISBN 981-02-0927-4.

Michler C. van Brummelen E. H., Hulshoff S. J., and de Borst R. (2003). The relevance of conservation for stability and accuracy of numerical methods for fluid–structure interaction. Computer Methods in Applied Mechanics and Engineering, 1 92(37–38), 4195–4215. doi: 10.1016/S0045-7825(03)00392-X.

Needleman L. (2014). Update on the lower extremity venous ultrasonography examination. Radiologic clinics of North America. 52(6):1359–1374.

Ozkucuk I. (2017). Quasi-Newton and artificial compressibility based partitioned algorithms for strongly coupled fluid structure interactions, Master Thesis, Istanbul Technical University. http://hdl.handle.net/11527/15722.

Parimi U. (2010). Computational Fluid Dynamics Analysis of Deep Veins with Focus on Deep Vein Thrombosis (DVT), University of Texas at El Paso. http://engineering.utep.edu/mu3com/ Publications/Thesis/U.Parimi.pdf.

Pedley T. J. (1980). The Fluid Mechanics of Large Blood Vessels, Cambridge University Press. XV, 446 S., ISBN 9780511896996.

Perktold K. and Rappitsch, G. (1995). Computer simulation of local blood flow and vessel mechanics in a compliant carotid artery bifurcation model. Journal of Biomechanics, 28(7), 845 856. https://doi.org/10.1016/0021-9290(95)95273-8.

Quriel K. Roy K. Greenberg, Richard M. Green, James M. Massullo, and Debra R. Goines. (1999). Volumetric index for the quantification of deep venous thrombosis, Journal of Vascular Surgery, 30(6): 1060-1066, doi: 10.1016/S0741-5214(99)70044-3.

Sankar D., Nagar A. K. and Vanav kumar A. (2015). Mathematical Analysis of Single and Two Phase Flow of Blood in Narrow Arteries with Multiple Contrictions. *Journal of Applied Fluid Mechanics*, *8*(4), 871–883. doi: 10.18869/acadpub.jafm.67.223.23336.

Syedah Salwa A. (2017). Predicting Thrombus Formation in Patients with Internal Carotid Artery Webs, University of Calgary. doi: 10.11575/ PRISM/27407.

Vierendeels J., Lanoye L., Degroote J. and Verdonck P. (2007). Implicit coupling of partitioned fluid–structure interaction problems with reduced order models. Computers & Structures, 85(11 14), 970–976. doi: 10.1016/j.compstruc.2006.11.006.

Wang C., Baker B. M., Chen C. S., Schwartz M. A. (2013). Endothelial cell sensing of flow direction. Arter. Thromb. Vasc. Biol., 33(9):2130–2136.

Weller H. G., Tabor G., Jasak H. and Fureby C. (1998). A tensorial approach to computational continuum mechanics using object-oriented techniques. Computers in Physics, 12(6), 620. doi: 10.1063/1.168744.

Willcox K. and Peraire, J. (2002). Balanced model reduction via the proper orthogonal decom-position. AIAA Journal, 40(11), 2323–2330. doi: 10.2514/3.15326.

Wu W. T., Aubry N. and Massoudi M. (2013). Channel flow of a Mixture of granular materials and a fluid. *ASME* International Mechanical Engineering Congress and Exposition, Proceedings (IMECE), 7A (November 2013). doi: 10.1115/IMECE2013-65385.